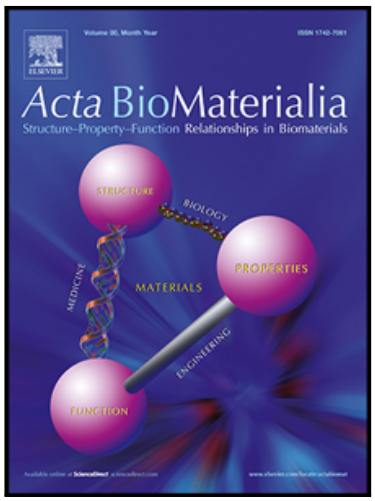

Sustained Delivery of a Heterodimer Bone Morphogenetic Protein-2/7 via a Collagen Hydroxyapatite Scaffold Accelerates and Improves Critical Femoral Defect Healing

Yang Liu , Manoj Puthia , Eamon J. Sheehy , Ines Ambite , Jikta Petrlova , Sujeethkumar Prithviraj , Maria Wimer Oxborg , Sujeesh Sebastian , Corina Vater , Stefan Zwingenberger , André Struglics , Paul E. Bourgine , Fergal J. O'Brien , Deepak Bushan Raina

PII: S1742-7061(23)00164-2
DOI: https://doi.org/10.1016/j.actbio.2023.03.028
Reference: ACTBIO 8657

To appear in: *Acta Biomaterialia*

Received date: 2 November 2022
Revised date: 14 March 2023
Accepted date: 20 March 2023

Please cite this article as: Yang Liu , Manoj Puthia , Eamon J. Sheehy , Ines Ambite , Jikta Petrlova , Sujeethkumar Prithviraj , Maria Wimer Oxborg , Sujeesh Sebastian , Corina Vater , Stefan Zwingenberger , André Struglics , Paul E. Bourgine , Fergal J. O'Brien , Deepak Bushan Raina , Sustained Delivery of a Heterodimer Bone Morphogenetic Protein-2/7 via a Collagen Hydroxyapatite Scaffold Accelerates and Improves Critical Femoral Defect Healing, *Acta Biomaterialia* (2023), doi: https://doi.org/10.1016/j.actbio.2023.03.028

Sustained Delivery of a Heterodimer Bone Morphogenetic Protein-2/7 via a Collagen Hydroxyapatite Scaffold Accelerates and Improves Critical Femoral Defect Healing

Yang Liu[1], Manoj Puthia[2], Eamon J. Sheehy[3,4,5], Ines Ambite[6], Jikta Petrlova[2], Sujeethkumar Prithviraj[7,8], Maria Wimer Oxborg[1], Sujeesh Sebastian[1], Corina Vater[9], Stefan Zwingenberger[9], André Struglics[1], Paul E. Bourgine[7,8], Fergal J. O'Brien[3,4,5], Deepak Bushan Raina[1,*]

1. The Faculty of Medicine, Department of Clinical Sciences Lund, Orthopedics, Lund University, 221 84 Lund, Sweden
2. The Faculty of Medicine, Division of Dermatology and Venerology, Lund University, 221 84 Lund, Sweden
3. Tissue Engineering Research Group, Department of Anatomy and Regenerative Medicine, Royal College of Surgeons in Ireland, University of Medicine and Health Sciences, 123 St. Stephens Green, Dublin, Ireland
4. Advanced Materials & Bioengineering Research (AMBER) Centre, RCSI, 123 St. Stephen's Green, Dublin 2, Ireland
5. Trinity Centre for Biomedical Engineering, Trinity Biomedical Sciences Institute, Trinity College Dublin, Dublin, Ireland
6. The Faculty of Medicine, Department of Laboratory Medicine, Division of Microbiology, Immunology and Glycobiology, Lund University, 221 84 Lund, Sweden
7. Cell, Tissue & Organ engineering laboratory, BMC B11, 221 84, Department of Clinical Sciences Lund, Stem Cell Centre, Lund University, Lund, Sweden
8. Wallenberg Centre for Molecular Medicine, Lund University, Lund, Sweden
9. University Hospital Carl Gustav Carus at Technische Universität Dresden, University Center of Orthopedics, Trauma and Plastic Surgery, 01307 Dresden, Germany

* Corresponding Author

Deepak Bushan Raina

BMC C12, Klinikgatan 28

221 84 Lund, Sweden

e-mail: deepak.raina@med.lu.se

Abstract

Despite the glimmer of hope provided by the discovery and commercialization of bone morphogenetic protein-2 (BMP-2) as a bone graft substitute, side effects related to the use of supraphysiological doses have hindered its clinical usage. In this study, we compared the osteoinductive potential of BMP-2 homodimer with a heterodimer of BMP-2/7, both delivered via a collagen-hydroxyapatite (CHA) scaffold delivery system, with the aim to reduce the overall therapeutic BMP doses and the associated side-effects. We first show that the incorporation of hydroxyapatite in collagen-based BMP delivery systems is pivotal for achieving efficient BMP sequestration and controlled release. Using an ectopic implantation model, we then showed that the CHA+BMP-2/7 was more osteoinductive than CHA+BMP-2. Further evaluation of the molecular mechanisms responsible for this increased osteoinductivity at an early stage in the regeneration process indicated that the CHA+BMP-2/7 enhanced progenitor cell homing at the implantation site, upregulated the key transcriptomic determinants of bone formation, and increased the production of bone extracellular matrix components. Using fluorescently labelled BMP-2/7 and BMP-2, we demonstrated that the CHA scaffold provided a long-term delivery of both molecules for at least 20 days. Finally, using a rat femoral defect model, we showed that an ultra-low dose (0.5 μg) of BMP-2/7 accelerated fracture healing and performed at a level comparable to 20-times higher BMP-2 dose. Our results indicate that the sustained delivery of BMP-2/7 via a CHA scaffold could bring us a step closer in the quest for the use of physiological growth factor doses in fracture healing.

Keywords: Bone morphogenetic protein, Collagen-hydroxyapatite, Controlled delivery, Fracture Healing, Heterodimer

Introduction

Bone transplantation is a routine surgical procedure that about 2-3 million individuals undergo every year [1, 2]. Traditional transplantation techniques involving the use of auto- and allograft materials have well documented drawbacks. As an alternative, research on bone tissue engineering (BTE) approaches have burgeoned during the past decade [3, 4]. Several attempts at mimicking the microstructural and physio-chemical composition of bone using laboratory-developed biomaterials have been made but the translational success has been limited due to the lack of inherent biological cues provided by the biomaterials at the defect site [5, 6]. Another potential pillar of the BTE framework is to combine biomaterials with cells that can differentiate into bone forming cells. To achieve this, the use of exogenously added mesenchymal stromal cells (MSCs) combined with biomaterial scaffolds has been seen as a promising strategy [7]. The clinical translation of this approach has been lagging for multiple reasons [8]. Most importantly, cells lose viability upon transplantation and often need to be modified to achieve desired therapeutic effects, raising questions regarding patient safety [9]. To overcome the aforementioned limitations associated with biomaterial scaffolds and cell therapy, a paradigm shift has lately been observed in the BTE approach [10]. Increasingly more research has been conducted on exogenously added signaling molecules to biomaterial scaffolds. Addition of the appropriate signaling molecules can lead to recruitment, activation, and differentiation of tissue healing cells in the host – thus negating the need to add cells to the scaffold prior to implantation [11].

Bone morphogenetic proteins (BMPs), particularly BMP-2 and BMP-7, are cytokines that aid in the chemotaxis and the differentiation of progenitor cells into bone forming cells and have been clinically used in patients undergoing bone reconstruction [12, 13]. The molecules are required to be delivered locally at the injury site, due to a short biological half-life, lasting only a few minutes. Combining BMPs with biomaterial scaffolds has been a rapidly growing field and studies have indicated that controlled and spatio-temporal delivery of BMP-2 and 7 is a pre-requisite to achieve desirable results. Yet, the only currently available market product, approved by the Food and Drug Administration (FDA) for use as a synthetic bone graft substitute is the homodimer BMP-2 protein delivered via an absorbable collagen sponge (ACS). The introduction of homodimer BMP-2 in clinical use has been tumultuous, from once being considered the Holy Grail in orthopedics to garnering skepticism due to associated drawbacks such as risk of heterotopic ossification, increased risk of cancer and local inflammation [14]. Most of the drawbacks associated with the usage of BMP-2 have been linked to the supraphysiological doses of the protein, which in many clinical cases has been reported to be as high as 1.5 mg/cm^3. We and others have demonstrated that the aforementioned side-effects caused by high dose BMP-2 delivery are a consequence of inefficient spatio-temporal delivery of the protein by the currently approved collagen sponge [15, 16]. It is therefore desirable to achieve a therapeutic effect from osteoinductive growth factors at doses that resemble the physiological growth factor concentrations present at the fracture site or discover/engineer novel osteoinductive factors with higher potency. One candidate is a heterodimer of BMP-2/7, which contains one subunit each from BMP-2 and BMP-7. In-vitro studies have indicated that the heterodimer BMP-2/7 is more efficient in inducing osteogenic differentiation of progenitor cells/MSCs than each of the respective homodimers [17]. These in-vitro findings are also supported by a small

number of in-vivo bone healing studies [18-20], but a direct in-vivo comparison of the osteoinductive properties of the currently used BMP-2 homodimer vs. the heterodimer BMP-2/7 have not been studied elaborately. Furthermore, little is known about the cellular and molecular events associated with the use of BMP-2/7 that impart it with a higher potency compared with BMP-2.

In light of the existing data, we hypothesized that the heterodimer BMP-2/7 would be more osteoinductive than the clinically used BMP-2 homodimer, both at ectopic and orthotopic locations. By virtue of this enhanced osteoinductivity, we hypothesized that it would be possible to use an ultra-low dose of BMP-2/7 for the healing of a critical long bone defect. To test this hypothesis, we used a well characterized bone-mimicking collagen-hydroxyapatite (CHA) based delivery system, with proven regenerative capacity, for the local delivery of both of these osteoinductive molecules [21]. The CHA scaffold is produced by controlled cooling of a slurry of collagen type I and hydroxyapatite (HA) followed by freeze drying and dehydrothermal crosslinking. The combined approach of HA incorporation and crosslinking has been shown to enhance the compressive stiffness of CHA scaffolds compared to non-crosslinked collagen scaffolds (4 kPa vs. 0.4 kPa) [22]. Controlled cooling leads to a uniform and interconnected porous structure congenial for cell attachment and survival. The HA component in the CHA scaffold not only helps in mimicking the composition of bone but studies have shown that it can potentially aid in sequestering biologically active molecules via electrostatic interactions [23-25]. The aims of this study were thus to: 1) investigate the potential of hydroxyapatite incorporation in a collagen scaffold to enhance BMP delivery; 2) perform a direct comparison of the osteoinductive potential of BMP-2 and BMP-2/7 delivered using a CHA scaffold in a “non-osseous” environment

using an established ectopic muscle pouch model; 3) compare the early differences in the cellular and molecular events that occur with the use of BMP-2 and BMP-2/7 as well as evaluate the genetic and biochemical composition of the neo-tissue; 4) evaluate the in-vitro and in-vivo release kinetics of BMP-2 and BMP-2/7 delivered using the CHA delivery system and; 5) compare the efficacy of using an ultra-low dose growth factor delivery using the CHA scaffolds in healing of a critical sized femoral defect in rats.

Materials and Methods

Study design

This study is divided into 4 main parts. Firstly, we investigated the potential of hydroxyapatite incorporation in a collagen scaffold to enhance prolonged BMP delivery. We then investigated the osteoinductive properties of BMP-2/7 delivered via a collagen-hydroxyapatite (CHA) scaffold and compared it with BMP-2 in an ectopic muscle pouch model. In the same model, we used an early time point in the regeneration process to evaluate the cellular, biochemical, and genetic events that occur with the use of these two osteoinductive factors. The release kinetics of BMP-2/7 and BMP-2 from the CHA scaffold was then studied both in-vitro and in-vivo. Finally, the ability of an ultra-low dose of both BMP-2/7 and BMP-2 delivered via a CHA scaffold was tested in a critical femoral defect model in rats.

Methods

Role of hydroxyapatite incorporation in collagen scaffolds for BMP delivery

Scaffold preparation

CHA scaffolds were prepared as previously described [22] and detailed methodology used during the fabrication of the CHA scaffolds is provided as supplementary information. The presence of HA in the CHA scaffold was verified using energy dispersive X-ray (EDX) analysis as well as x-ray diffraction (XRD) analysis. The methodology used for EDX and XRD analysis is provided in the supplementary information. The degradation rate of the CHA scaffold was also studied in phosphate buffered saline (PBS) at 37 °C over a period of 5-weeks by evaluating the change in weight of the scaffold according to previous protocols [15]. Absorbable collagen sponge (ACS) without hydroxyapatite (HA) was used from the Medtronic® Infuse Bone Graft Kit (Medtronic, Ireland). In order to study the structural characteristics of CHA and ACS scaffolds, 4 mm diameter (Ø) scaffolds were embedded in liquid paraffin at 65 °C and sectioned to 20 μm thickness using a semi-automatic microtome (Thermo Scientific, U.S.A). In order to verify the presence and distribution of HA particles in the scaffolds, sections collected on glass slides were deparaffinized using xylene, rehydrated with decreasing EtOH gradient and deionized water before staining with 2% w/v Alizarin Red S (Sigma Aldrich, U.S.A) at a pH of 4.2. Stained slides were cleared in xylene and mounted before being digitized using a Hamamatsu nanozoomer slide scanner. Scaffold sections were also analyzed using a scanning electron microscope (Jeol, Japan) by mounting them on 8 mm Ø cover slips, deparaffinized using xylene and sputter coated before imaging at 3 kV operating voltage.

Interaction between BMP-2 and HA

In order to compare the binding of BMP-2 to the ACS and CHA scaffolds, BMP-2 (R&D systems, U.S.A) was first fluorescently labelled with VivoTag 680XL protein labelling kit (Perkin Elmer, U.S.A) following the manufacturer's guidelines. Protein concentration

before and after the labelling procedure was carried out using a nanodrop (Thermo Scientific, U.S.A) in order to quantify protein recovery after labelling. Sections of both ACS and CHA scaffolds (n=5) mounted on glass slides were deparaffinized and rehydrated after which they were incubated with 5 μL of the fluorescently-labelled protein (0.18 μg) for 10 min at room temperature following which the slides were washed by dipping the slides in deionized water for 10 s. Protein amount was optimized in order to ensure robust fluorescence quantification without the background interference that generally occurs with in-vivo imaging system (IVIS) imaging at high labelled protein concentrations. The sections were then air dried and mounted using a xylene based mounting medium. The slides were imaged on an IVIS scanner (Perkin Elmer, U.S.A) and the fluorescence in the respective scaffolds was quantified using Living Image 4.0 Software (PerkinElmer). ACS and CHA scaffolds without any protein were used as negative controls.

The interaction between BMP-2 and HA was further studied using circular dichroism (CD) spectroscopy. CD measurements were performed on a Jasco J-810 spectropolarimeter (Jasco, USA) equipped with a Jasco CDF-426S Peltier set to 25 °C. The BMP-2 (R&D Systems, U.S.A, carrier free) was diluted to 2 μM in buffer (Tris 10 mM, 4 mM HCl, pH 7.4) and incubated with or without micro HA particles (Plasma Biotal, Tideswell, UK) 1:1 and 1:5 ratio (w:w) for 30 min at 25 °C, placed in a 1 mm quartz cuvette and, after extensive purging with nitrogen, scanned over the wavelength interval 190–260 nm (scan speed: 20 nm/min). We calculated the averages of five scans for each sample. The baseline (10 mM Tris, 4 mM HCl, pH 7.4, and HA) was subtracted from the spectra of each sample. Finally, native gel analysis was also performed to confirm the interactions between BMP-2 and HA using Blue BN-PAGE and Western blot analysis. BMP-2 (2 μM) was incubated with HA (1:5) for 30 min at 25°C. The samples

(0.25 µg per well) were loaded under non-reducing conditions on BN-PAGE (NativePAGE Bis-Tris Gels System 4-16%, Invitrogen) according to the manufacturer's instructions, which were followed by Western blotting. The membrane was incubated with mouse anti-human BMP-2 (cat#ab119581, Abcam), at a concentration of 1:1000 in 5% fat-free milk in PBS-T, overnight at 4°C. The high-molecular weight complexes of BMP-2 were then detected using a secondary rabbit anti-mouse polyclonal antibody that was conjugated to HRP (cat#P0260, Dako) (diluted 1:2000 in PBS-T complemented with 5% milk) after incubation for 30 min at room temperature. The bands were revealed by incubating the membrane in the developing substrate (Super Signal West Pico PLUS Chemiluminescent Substrate, cat#34580, Thermo Scientific). Signal was acquired by a Chemi-Doc (Bio-Rad) system. All the experiments were performed at least three times.

Comparison of the osteoinductivity of BMP-2/7 and BMP-2 delivered via a CHA scaffold in an ectopic muscle pouch model in rats

For muscle pouch implantation, a 6 mm diameter (Ø) biopsy punch was used to cut CHA scaffold cylinders of 7 mm height, disinfected in 70% EtOH for 1 h with two changes, washed with 99.5% EtOH for 15 min and finally washed 3X with PBS for 10 min each. At the end of the washing steps, the excess PBS was removed carefully using a pipette tip. The final size of the CHA scaffolds after the removal of excess liquid was approximately 4 mm Ø and 5 mm height. During the animal experimentation, 3 different doses of BMP-2/7 (R&D Systems, U.S.A) and 4 different doses of BMP-2 (R&D systems, U.S.A and from the clinically approved Medtronic® InductOS kit, Medtronic, Ireland) reconstituted in 4 mM hydrochloric acid were used. Protein loading was carried out by soak loading of the protein on each scaffold for at least 30 min at room temperature prior to implantation in the animal. Volume of the protein solution loaded on the scaffolds was chosen

appropriately to ensure that the scaffold was thoroughly soaked with the protein solution without any leakage.

Study design, protein loading and surgical procedure

A total of 13 Sprague-Dawley rats (male, average weight: 330±30 g) were used in this experiment and the animals were divided into two groups of n=8 and n=5 based on the type of the protein used (Supplementary Figure 1A). The detailed surgical procedure describing this animal model is published elsewhere [26]. In the first set of 8 animals, 2 muscle pouches were created on either side of the abdominal midline and a CHA scaffold containing either 0.2 µg or 2 µg of BMP-2/7 (R&D Systems, U.S.A) were implanted. In the remaining 5 animals, the two pouches contained CHA scaffolds loaded with 0.2 µg or 2 µg of BMP-2 (R&D Systems, U.S.A). In the 2 µg group, 20 µg BMP-2/7 or BMP-2 was reconstituted in 100 µL of PBS containing 4 mM HCl leading to a protein concentration of 0.2 mg/mL. From this solution, 10 µL of the respective protein solutions containing 2 µg of the protein was loaded onto each CHA scaffold. For the 0.2 µg groups, 10 µL of 0.2 mg/mL stock solution was diluted in 90 µL PBS (containing 4 mM HCl) to obtain a 0.02 mg/mL solution. 10 µL of the protein solution containing 0.2 µg protein was then used for each scaffold. Protein amounts were chosen based on an earlier report wherein 2 µg BMP-2 was the lowest reported dose to successfully lead to bone formation in an ectopic muscle pouch model in rats [27] and the 10-times lower dose of 0.2 µg was chosen as a low dose control. The experiment was terminated at 4-weeks by sacrificing the animals using CO_2 asphyxiation. All specimens were harvested, fixated in 4% formalin and subjected to micro-CT followed by histological analysis.

Evaluation of bone formation at 4-weeks using micro-CT and histology

Micro-CT analysis was performed on a MILabs U-CT system (Utrecht, Netherlands) with an X-ray energy of 65 kV and 75 µA current using the ultra-focus mode with a voxel size of 20 µm. Two hydroxyapatite phantoms with densities corresponding to 0.25 and 0.75 g/cm^3 were also scanned for density calibration. For quantification of bone volume (BV), reconstructed images from individual samples were imported into Seg3d2 (University of Utah, U.S.A) and a density threshold of 0.45 g/cm^3 was applied to quantify BV and to produce the 3D reconstructions. Post micro-CT, samples were decalcified using 10% neutral buffered EDTA at 4 ºC for 2-weeks, embedded using routine paraffin procedures and sectioned to a thickness of 5 µm using a microtome (Thermo Scientific, U.S.A). Tissue sections were stained with hematoxylin and eosin (H&E), digitized using a Hamamatsu (Hamamatsu Photonics, Japan) slide scanner and imported into a histomorphometry software (HALO™, Indica Labs, U.S.A) for semi-automatic quantification of new bone area.

Early comparison of progenitor cell homing, biochemical and histological composition and the genetic signature of the neo-tissue formed by CHA scaffolds loaded with BMP-2/7 and BMP-2

Study design and protein loading

A total of 20 Sprague-Dawley rats (male, average weight: 388±42 g) were used in this experiment and comparison of treatments was performed in a pairwise fashion to minimize inter-animal biological variation. A previously described abdominal muscle pouch model was used to conduct these experiments with a difference that 3 pouches were created in each animal and the animals were sacrificed at day 10 post implantation. All 20 animals received three implant materials; 1) CHA scaffold, 2) CHA+BMP-2/7 (0.5 µg/scaffold) and 3) CHA+BMP-2 (0.5 µg/scaffold) each separated by

a minimum distance of 2 cm from the other. CHA scaffolds containing BMP molecules were loaded with 10 µL of the protein solution. In brief, each protein was resuspended in 4 mM HCl containing PBS to a final concentration of 0.2 mg/mL. 50 µL of the stock solution was diluted with 150 µL PBS to produce a protein solution containing 0.05 mg/mL protein. 10 µL of this solution was added to each scaffold before implantation.

Analysis of progenitor cell homing using flow cytometry

The experiment on progenitor cell homing was carried out using flow cytometry (FACS). Samples from a total of n=7 animals were used for this experiment. Harvested neo-tissue specimens were carefully cleaned of the muscle tissue and digested in an enzyme cocktail to obtain a cell suspension. More detailed protocol is provided in supplementary information. The cells from the digested tissues were centrifuged at 1500 rpm for 5 min, the supernatant was discarded, and the cells were resuspended in 1 mL FACS buffer (PBS with 2% v/v FCS, 2 mM EDTA), stained with crystal violet and counted using Biorad TC20™ cell counting slides (Bio-Rad, Sweden). The cell suspension was re-spun to form a cell pellet, which was resuspended in 100 µL FACS buffer after which all primary antibodies (see supplementary table 4) were added to the cell suspension and incubated at 4 ºC for 1 h. Antibody dilutions were added to compensation beads for setting up fluorescence compensation (UltraComp eBeads™ compensation beads, Thermofisher Scientific, U.S.A). At the end of incubation, cells were centrifuged, and the supernatant was discarded. The cell pellet was washed with 1 mL FACS buffer, centrifuged, and re-suspended in 100 µL FACS buffer following which the respective secondary antibodies were added (see Supplementary Table 4). Cells were incubated with the secondary antibody for 1 h at 4 ºC, centrifuged and washed with 1 mL FACS buffer, and resuspended in 350 µL FACS buffer containing nuclear stain

DAPI (500 ng/µL). The cells were then analyzed on a BD LSRFortessa™ cell analyzer (BD, U.S.A). The gating strategy used for the experiment is provided in Supplementary Figure 2.

Biochemical assessment of neo-tissue constructs

Quantification of glycosaminoglycans (GAGs) was performed using a modified Alcian blue assay [28, 29] while total collagen content in the form of hydroxyproline measurements were performed using a commercially available assay (Sigma Aldrich, U.S.A). Sample preparation was performed according to previous studies [29] and protein extraction was performed using guanidinium hydrochloride (Gua-HCl). The non-soluble proteins mainly comprising of collagens formed a visible pellet after centrifugation (Gua-Pellet), which was stored at -20 ºC for hydroxyproline content measurement. The soluble protein fraction was precipitated using ice-cold EtOH solution comprising of 95% EtOH and 50 mM sodium acetate overnight at 4 ºC. The precipitate was then collected by centrifugation while the supernatant was discarded. Precipitated protein pellet was re-suspended in Tris-acetate buffer (pH 7.6, 50 mM Tris-acetate, 50 mM sodium acetate) followed by another round of precipitation for 4 h. Finally, the protein pellet was solubilized in Tris-acetate buffer and used for the Alcian blue assay (detailed assay methodology is provided in the supplementary information). GAG concentration/well was calculated from the standard curve and was expressed as GAG/tissue as well as GAG/mg tissue. Any specimens that had a GAG concentration under the lower limit of quantification (LLOQ) was assigned an imputed value, which equated to LLOQ/2 based on earlier studies [30]. The LLOQ was chosen to be the lowest point on the standard curve where GAG recovery was ≧85%. For the measurement of hydroxyproline content, Gua-Pellet collected above was suspended in

12 M HCl and hydrolyzed overnight at 120 ºC after which manufacturers guidelines (Sigma-Aldrich, Kit# MAK008, U.S.A) were followed to quantify the total hydroxyproline content/tissue as well as hydroxyproline/ mg tissue.

Transcriptomic characterization of the neo-tissue

Transcriptomic analysis was performed on n=3 specimens for the BMP-2/7 and BMP-2 treated neo-tissue, respectively and n=2 for CHA only controls. For RNA extraction, all specimens were homogenized in RLT buffer (Qiagen RNeasy, Qiagen, Germany) with 1% β-mercaptoethanol, using hard tissue grinding tubes (CK28 Precellys Lysing Kit, Bertin, France) on a Qiagen tissue homogenizer for 5 min. Total RNA extraction was performed using the RNeasy Mini Kit (Qiagen) and on-column DNase digestion, following the manufacturers guidelines. RNA was subjected to expression microarray analysis: 100 ng of total RNA were amplified using the Affymetrix WT PLUS Reagent Kit (Thermo Fisher Scientific) and hybridized, using the GeneTitan system, onto Clariom S Rat arrays (16 h at 45 °C). Transcriptomic data was normalized using the Robust Multi-chip Analysis (RMA) algorithm implemented in the Transcriptome Analysis Console software (TAC v.4.0.1.36, Applied Biosystems, ThermoFisher Scientific). The TAC software calls the limma differential expression portion of the Bioconductor package to provide fold change. Relative expression was analyzed by ANOVA using the empirical Bayes (eBayes) method and genes with a p-value <0.05 and an absolute fold change >2.0 were considered differentially expressed. Heat-maps were constructed using the Prism 9 software. Differentially expressed genes and regulated pathways were analyzed using Ingenuity Pathway Analysis software (IPA, Qiagen), using right-tailed Fisher's Exact test.

Histological characterization of the neo-tissue

Finally, to characterize the early neo-tissue characteristics, specimens (n=2) were embedded in paraffin, cut, and collected on glass slides, and stained with Safranin O/Fast green as well as hematoxylin and eosin.

Analysis of the release kinetics of BMP-2/7 and BMP-2 from ACS and CHA scaffolds

The in-vitro release kinetics of both BMP-2/7 and BMP-2 was performed using an enzyme linked immunosorbent assay (ELISA) by following the manufacturers guidelines (Abcam, U.K). A total of 2 µg of both BMP-2/7 and BMP-2 were initially loaded on the ACS and CHA scaffolds (n=5 for each protein, samples were run as singlets) after which they were incubated with 1 mL PBS at 37 °C. PBS was collected and replenished at pre-determined time intervals. Protein release was quantified in the supernatants, which were kept frozen at – 20 °C until the day of assay.

In-vivo release of both BMP molecules was studied by using fluorescently labelled BMP-2 and BMP-2/7 (VivoTag 680 NIR, Perkin Elmer, U.S.A). Experiment on the in-vivo release kinetics was only performed using CHA scaffolds. 10 µL of the respective fluorescently labeled protein solutions (protein amount BMP-2/7=1.6 µg/scaffold and BMP-2=1.8 µg/scaffold) were loaded on each CHA scaffold and the scaffolds were incubated for at least 30 min before implantation. To investigate the in-vivo pharmacokinetics of BMP-2 and BMP-2/7 in a surgical implantation situation, we used a mouse model of subcutaneous implantation. Fluorescently-labelled BMP-2 or BMP2/7 loaded CHA scaffolds were implanted in the sub-cutaneous tissue of BALB/c mice (8-10 weeks old, females; n=6 for each protein). Hair from the dorsum of the mice were trimmed and cleaned with 70% alcohol. Under isoflurane anaesthesia, an approximately

5 mm incision was made on the skin of the mouse's back and an implant with labelled (VivoTag 680 NIR) BMP-2 or BMP-2/7 was inserted under the skin. The skin opening was immediately closed with a single suture (VICRYL^{TM}, Johnson & Johnson, Belgium) and the mice were immediately returned to the cages. Detection and release of BMP-2 or BMP-2/7 was monitored using IVIS imaging in the fluorescence mode and the data was acquired and analyzed using Living Image 4.0 Software (PerkinElmer). Fluorescence signal from mice was acquired at 2 h, 24 h, 72 h, 6 d, 12 d and 20 days after the implantation and a region of interest (ROI) was drawn manually to quantify the signal.

Use of ultra-low dose BMP-2/7 delivered via a CHA scaffold for healing of a critical femoral defect in rats and comparison with BMP-2

Study design and surgical model

A previously described rat femoral defect model comprising of a 5-mm mid-diaphyseal bone defect was used in this study (Supplementary Figure 3) and the sample size in the control and experimental groups (Supplementary Table 5) were based on the results from the previous study [31]. The surgical procedure remained the same but instead of a metallic fixation device, we chose to use poly ether ether ketone (PEEK) plates as PEEK materials allow for detailed radiographic imaging of fracture healing using micro-CT without creating imaging artefacts. Surgical steps, animal care and a description of the fracture fixation system is provided in the methods section of the supplementary information as well as in Supplementary Figure 3.

A total of 49 Sprague Dawley rats (male, average weight: 365±14) were used for this experiment and the rats were divided into following experimental treatment groups: 1) CHA+BMP-2 (10 µg) (n=12), 2) CHA+BMP-2/7 (0.5 µg) (n=13) and 3) CHA+BMP-2 (0.5

µg) (n=12). Apart from the 3 experimental groups, we also chose to use 2 control groups comprising of: 1) Defect only (n=6) and 2) CHA scaffold only (n=6). Control groups comprised of fewer animals compared to the experimental group because in an earlier experiment we demonstrated that the empty group or the biomaterial alone is not sufficient for healing of these types of critical defects [31]. For growth factor loading, BMP-2 (Medtronic®, Infuse Bone Graft Kit, Ireland) was reconstituted as a 1 mg/mL solution in 4 mM HCl containing PBS. 10 µL of this stock solution were used for loading the CHA scaffold in the first treatment group containing 10 µg BMP-2. BMP-2 stock solution was diluted to 0.05 mg/ml and 10 µL of the diluted solution were pipetted on the CHA scaffolds in the treatment group containing 0.5 µg BMP-2. BMP-2/7 (R&D Systems, U.S.A) loaded scaffolds were prepared by diluting a 0.2 mg/mL stock solution of BMP-2/7 to 0.05 mg/mL solution and 10 µL of the diluted solution were loaded on the CHA scaffolds. In the defect only group, the femoral defect was left untreated while in the CHA only group, CHA scaffolds loaded with 10 µL of the buffer solution (PBS containing 4 mM HCl) were placed in the defect. Protein dose of 10 µg BMP-2 was chosen as a positive control standard dose as this is the most commonly reported BMP-2 dose in rat critical femoral defects [20]. The 0.5 µg BMP dose was chosen to represent an ultra-low dose based on the results from the muscle pouch experiments.

PET-CT based analysis of fracture healing at an early time point of 3-weeks

At t= 3-weeks post intervention, 3 animals in each treatment group (except empty group where n=2) were randomly chosen for PET-CT analysis. Animals were injected with Na-^{18}F (average radioactivity: 54±3.5 MBq) intraperitoneally followed by returning the animals to their respective cages. At t=30 min, the animals were anesthetized (isoflurane 2%, O_2 0.4 L/min) and a lower body CT scan (voltage=65 kV, exposure= 500

ms, zoom=maximum field of view, binning=1:1) was performed with an isotropic voxel size of 71 µm to localize the defect. The CT was then followed by a PET scan (at t=1 h) using default settings of the instrument (nano PET-CT, Mediso Medical Devices, Hungary) for Na-^{18}F tracer. CT and PET images were superimposed and a cylindrical ROI covering the entire defect region was drawn using an automatic quantification suite (VivoQuant 4.0, inviCRO, U.S.A) to quantify the total radioactive counts within the ROI (Supplementary Figure 4, Top). The counts were normalized to the ROI volume and the injected radioactivity for each animal and the data were presented as (counts/mm^3)/MBq injected radioactivity.

Micro-CT based analysis of fracture healing at early (4-weeks), intermediate (6 and 8-weeks) and late (12-week) healing phases

At 4, 6 and 8 weeks, all animals were subjected to in-vivo micro-CT (anesthetized as above) on a MiLabs U-CT micro-CT scanner and the images were reconstructed to 30 µm voxel size. At 12 weeks, ex-vivo imaging of the harvested bones was performed on the same instrument and the images were reconstructed to 20 µm voxel size. Bone volume (BV) was calculated in a 4.5 mm cylindrical ROI to avoid interference from the native cortical bone (Supplementary Figure 4, bottom). CT images from each time point were also used to determine radiographic union (defined as complete bridging of 3 out of 4 cortices in both sagittal and coronal planes) and the analysis was performed independently by a trained orthopedic surgeon who was blinded to the study design. The bi-planar CT images were also used to assign a radiographic healing score based on the modified RUST protocol [32]. After the radiographic assessment was complete, the fixation plates from all specimens were carefully removed and judged for mechanical union by the 2 authors (MWO and DBR) of this study. A mechanical union was defined

as resistance to bending or rotation upon manual palpation and mechanically bridged samples were used for 3-point bending.

Mechanical properties of the regenerated bone at 12-weeks

Femurs with a defect and their respective contralateral femurs were subjected to 3-point bending using an established protocol [31]. In short, each specimen was placed on the bottom stage of a 3-point bending jig having its support points 16 mm apart. The loading nose and the two pillars on the resting stage both had a contact width of 1 mm. Samples were placed in the antero-posterior position and in the case of the femurs with a defect, care was taken to place the defect in the middle of the support points. The specimens were then loaded on an Instron load frame (Instron® 8511.20, Instron Corp., U.S.A) using a pre-load of 20 N for 10 s followed by axial compression at a ramp rate of 0.25 mm/s until fracture. Force-displacement curve was then used to extract the peak force to fracture data. Furthermore, slope of the linear region of the force-displacement curve was also used to compute stiffness while the area under the curve until the fracture point was used to compute work to fracture.

Histological characterization of the regenerated bone at 12-weeks

The remaining intact specimens after 3-point bending (n=2/group) from the 12-week time point were fixed in 4% formalin, decalcified in 10% w/v EDTA (pH 7.4, 4 ºC) for 4-weeks with fresh EDTA changes twice every week. Samples were then embedded in paraffin and cut to 5 µm thickness and stained with Masson's trichrome kit (Sigma Aldrich, U.S.A) using standard histological protocols. Slides were digitized using a Hamamatsu (Hamamatsu, NanoZoomer, Japan) slide scanner.

Sample exclusion

One sample each from the CHA+BMP-2/7 (2 μg and 0.2 μg) groups from the muscle pouch model was excluded from the histomorphometry analysis of new bone formation (Fig. 1B) due to erroneous sample preparation. One animal in the CHA+BMP-2 (10 μg) group had to be excluded after the 4-week time in the femur defect model because the animal was lost to follow-up due to anaesthesia complications developed during micro-CT imaging.

Statistics

Data are presented as mean±SD. Statistical analysis was performed on Prism 9 (GraphPad Inc, U.S.A). Data were checked for normality using the Shapiro-Wilk normality test and the Q-Q plots. Depending on the distribution of the data, comparison of data from two treatment groups observed in the same animal was performed using a paired sample t-test or Wilcoxon signed rank test. Data emanating from experiments involving the comparison of two groups without any biological dependence were tested using paired sample t-test or Mann-Whitney U test. Comparison of independent data generated from more than two treatment groups was compared using either ANOVA with Tukey's post-hoc test or the non-parametric variant (Kruskal-Wallis) of ANOVA with Dunnett's multiple comparison test. Statistical significance was set at $p<0.05$ in all experiments. Detailed description of the statistical tests used for each experiment are provided in supplementary table 6.

Animal ethics and welfare

Animal experiments were performed with due consent from the Swedish Board of Agriculture (Jordbruksverket) with following permit numbers: 1) 18-08106/2018 (femur defect), 2) 15288/2019 (muscle pouch model) and M5934-19, 8871-19 (subcutaneous mouse model). Animals were fed food and water *ad libitum* and maintained in a sterile environment with 12h dark/light cycles without any dietary alterations. All personnel handling and working with animals were trained and certified (FELASA) for work with animals and ARRIVE guidelines were followed during experimentation.

Results

Hydroxyapatite is pivotal for efficient BMP sequestration

To elucidate the importance of HA incorporation in collagen scaffolds for improved BMP sequestration and sustained delivery, we compared the BMP sequestration ability of the currently FDA-approved absorbable collagen sponge (ACS) with a collagen-hydroxyapatite (CHA) biomaterial. The presence of HA in the CHA scaffold could be clearly seen in the EDX and XRD spectra seen in supplementary figures 5 and 6. Both biomaterials (ACS and CHA) had a macroporous structure with pores ranging up to a few 100 micrometres (Fig. 1A).

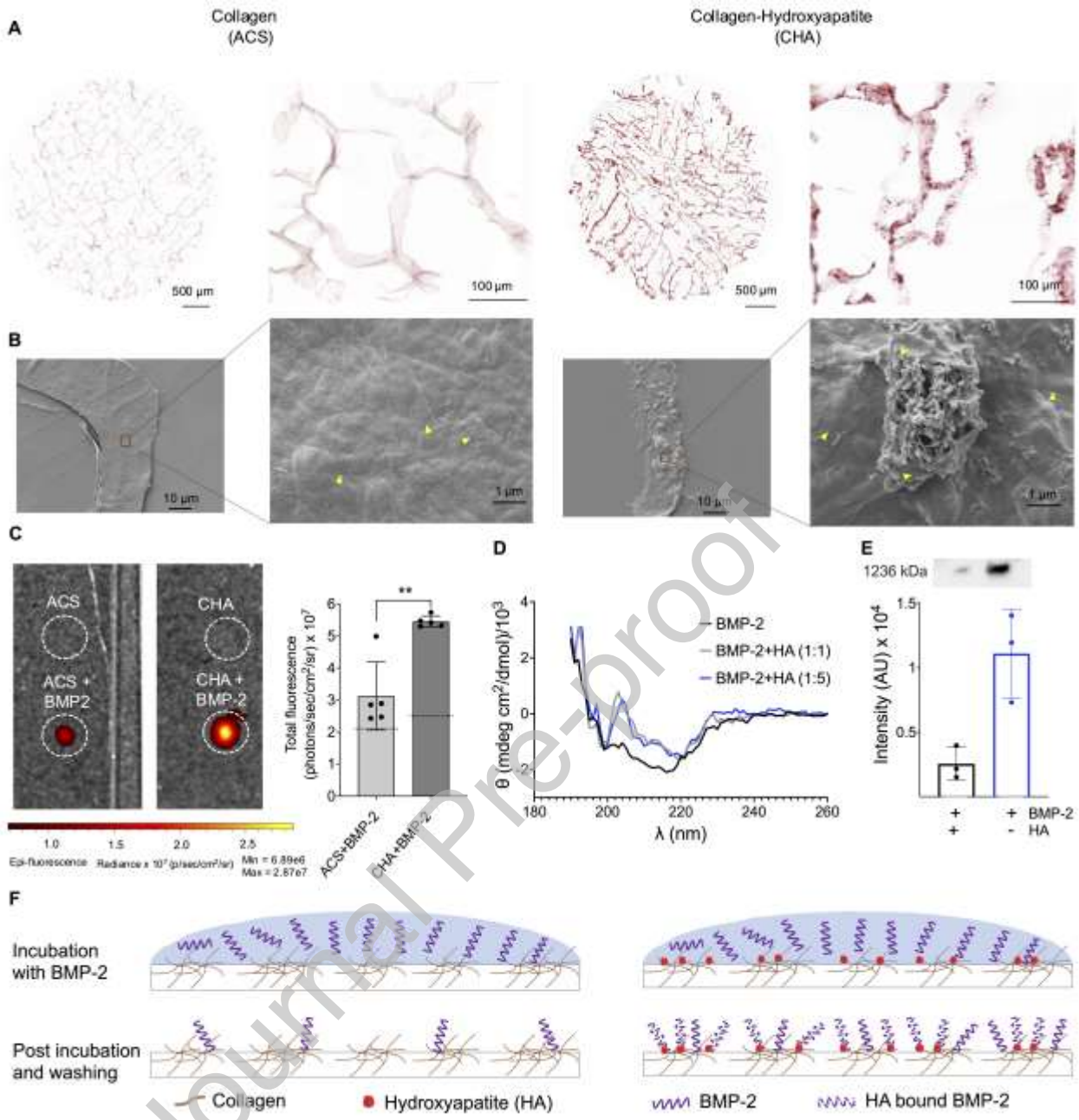

Figure 1: Structural characteristics of the absorbable collagen sponge (ACS) and the collage-hydroxyapatite (CHA) biomaterials and the role of hydroxyapatite (HA) incorporation on BMP sequestration. (A) Alizarin red stained 20 µm sections of ACS (left) and CHA (right) scaffolds. Notice the lack of calcium staining in the ACS scaffold and the presence of homogenously distributed HA particles (red dots) in the CHA scaffolds. (B) Scanning electron microscopy images of the scaffold walls in the ACS (the two left panels) and the CHA scaffold (the two right panels). Yellow arrows in the high magnification images emphasizes the fibrillar collagen type 1 present in both the scaffolds. Hydroxyapatite particles can be seen embedded in the collagen matrix in the

CHA scaffold at both low and high magnification. (C) In-vivo imaging system (IVIS) images of glass slides containing ACS, and CHA scaffold sections (20 μm) incubated with fluorescently labelled BMP-2 for 10 min followed by thorough washing to detect scaffold-BMP binding. Protein free specimens were used as background controls. Data in the bar graph presents the quantification of the fluorescence from the IVIS images (n=5 per group). (D) Circular dichroism (CD) spectra shows the β-sheet structures of BMP-2 protein, and the change of BMP-2 confirmation to α-helical structures after incubation with HA indicating BMP-HA binding. Data are presented as the mean ± SD of three independent experiments (n=4). (E) Western blot analysis (using an antibody against BMP-2) shows a decrease of higher molecular complexes of BMP-2 (2 μM) after incubation with HA 1:5 ratio (w:w) (n=3). The intensity of the bands representing high-molecular complexes of BMP-2 was measured as presented in the bar graph. (F) An illustration of BMP interaction with ACS (left), and CHA scaffold (right) based on the results obtained from the HA distribution experiments, IVIS imaging, CD spectroscopy and Western blot. ** indicates $p<0.01$, actual p-values are presented in Table S5.

The ACS material had an obvious lack of calcium staining due to the absence of the hydroxyapatite (HA) component, while the HA particles were homogenously distributed in the polymeric walls of the CHA scaffold (Fig. 1A). Scanning electron microscopy images of the scaffold walls verified the presence of fibrillar collagen structures in both ACS and CHA materials and the micro-HA particles in the CHA material were embedded in the fibrillar collagenous network (Fig. 1B). The interaction between BMP-2 and the ACS and CHA scaffolds was also studied using in-vivo imaging system (IVIS) by incubating the respective scaffolds with fluorescently labelled BMP-2 for 10 min followed by washing of the unbound protein. It was verified that the presence of HA in the CHA scaffolds significantly enhanced the retention of BMP-2 compared to pristine collagen scaffolds (Fig. 1C). To further verify that it was indeed the HA component in the CHA scaffolds that was responsible for improved BMP sequestration, we used circular dichroism (CD) spectroscopy to study the conformational changes in BMP-2 upon

interaction with HA. We detected a change in the secondary structure of the protein from β-sheet structures, a typical structural feature of aggregating proteins, to α-helical structures after exposure to HA, indicating BMP-HA binding. We observed two minima, which are typical for α-helical structures at 222 and 210 nm, noticed in both concentrations of HA (1:1 and 1:5) (Fig. 1D). Moreover, we analyzed images from blue native Western blot analyses showing that pure BMP-2 aggregates migrated in the native gel at around 1200 kDa as reported in the literature [33], but the interaction between BMP-2 and HA (1:5) prevented the BMP-2 from migrating in the gel and onto the membrane, verifying the interaction between BMP-2 and HA (Fig. 1E, F). Finally, in-vitro scaffold degradation assay indicated that nearly 35% of the CHA scaffold degraded over a period of 5-weeks (Supplementary figure 7).

BMP-2/7 delivered via a CHA scaffold is more osteoinductive than BMP-2

After establishing the importance of HA incorporation in collagen scaffolds and demonstrating the superiority of CHA scaffolds over ACS scaffolds in BMP sequestration, our next goal was to compare the osteoinductive potential of BMP-2/7 with the current gold-standard BMP-2 in an ectopic muscle pouch model. Due to the lack of a bone marrow niche along with its anatomical separation from bone, evaluation of osteoinductivity in this model is considered to be robust [34]. In general, CHA scaffolds treated with BMP-2/7 had a larger gross appearance than the BMP-2 treated specimens. Micro-CT imaging of the regenerated neo-tissue after 4-weeks of in-vivo implantation showed that the CHA scaffolds loaded with BMP-2/7 demonstrated a significantly higher bone volume compared with BMP-2 at both low (0.2 μg) and high (2 μg) doses (Fig. 2A, Supplementary Figure 1).

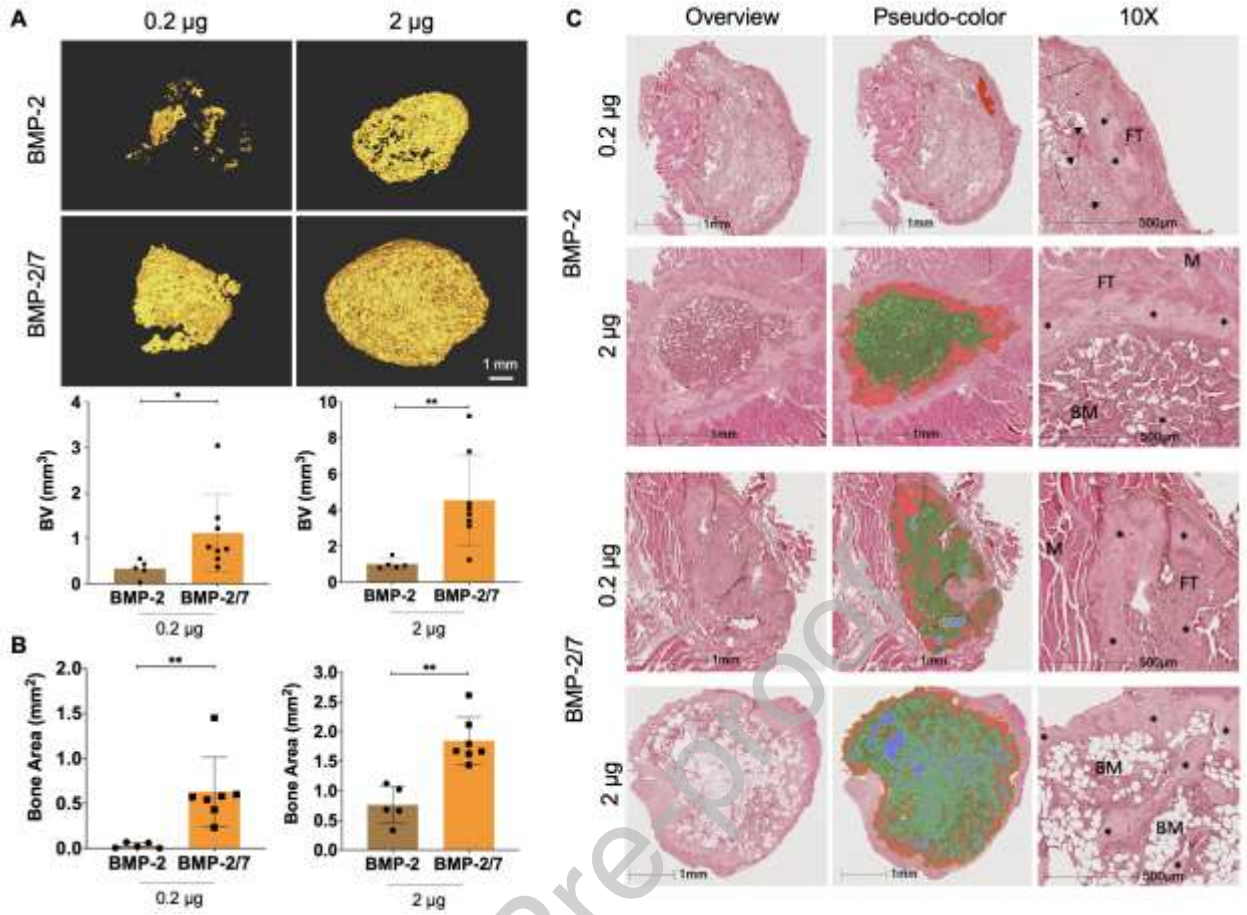

Figure 2: Comparison of the osteoinductive potential of BMP-2/7 and BMP-2 delivered via a collagen-hydroxyapatite (CHA) scaffold in the abdominal muscle pouch in rats. (A, top) Representative Micro-CT based 3D reconstructions of the bone tissue formed in the abdominal muscle pouch model, 4-weeks post implantation (images from all animals are presented in Fig. S1). (A, bottom) Quantification of the bone volume (BV) in the presence of both low dose (left) and high dose (right) BMP molecules delivered using the CHA scaffolds. In panel A, n=5 for BMP-2 group and n=8 for BMP-2/7 group. (B) Histology based histomorphometric quantification of bone area in the neo-tissue formed at 4-weeks using both low (left) and high (right) doses of BMPs. In panel B, n=5 for BMP-2 group and n=7 for BMP-2/7 group. (C) Representative hematoxylin and eosin stained neo-tissue sections from the muscle pouch model after 4-weeks of implantation. Red color in the pseudo-colored images indicates new bone tissue, green shows bone marrow and fibrous tissue and blue shows the glass surface. High magnification images verify the presence of bone tissue (*), fibrous tissue (FT), muscle tissue (M), bone marrow (BM) and remnants of the CHA scaffold (arrow). Data is presented as

mean±SD. * indicates p<0.05 and ** indicates p<0.01, actual p-values are presented in Table S5.

Histological analysis corroborated with the micro-CT results and indicated that the harvested tissue was larger in the BMP-2/7 treated CHA specimens (Fig. 2B, C). Significantly more new bone area was observed in the BMP-2/7 loaded CHA scaffolds compared with the BMP-2 treated scaffolds, irrespective of the protein dose.

BMP-2/7 loaded CHA scaffolds demonstrate enhanced progenitor cell homing and accelerated cartilage/bone formation from an early stage

Progenitor cell (cell populations identified in heterotrophic ossification specimens and endosteal lining of long bones capable of efficient tri-lineage differentiation) homing capabilities of CHA scaffold-BMP-2/7 combination was used as a surrogate for unraveling the early cellular events that occurred with BMP-2/7 treatment. Progenitor cell population markers were established based on earlier studies [35-37], and an intermediate growth factor dose (0.5 μg) was chosen based on the results above (Fig. 2). Compared with BMP-2, BMP-2/7 loading of CHA scaffolds significantly enhanced the progenitor cell homing in the implanted scaffolds/neo-tissue construct at day-10 (Fig. 3A, Supplementary Figure 2). Representative images using Safranin O/Fast green and hematoxylin and eosin staining indicated that the BMP-2/7 loaded CHA scaffolds presented with more cartilage and bone tissue after 10-days of in-vivo implantation compared to CHA+BMP-2 scaffolds implanted in the same animal (Fig. 3B). Histology findings were also supported by the quantitative biochemical characterization of the newly formed tissue. The total glycosaminoglycan (GAG) content/tissue as well as total hydroxyproline/tissue were significantly higher in the BMP-2/7 loaded CHA scaffolds in comparison with BMP-2 treated CHA scaffolds (Fig. 3C). However, no difference in GAG

or hydroxyproline density (total content normalized to tissue weight) were observed between the two groups indicating that the differences in GAG and hydroxyproline content likely emanates from the differences in the tissue volume rather than density of the extracellular matrix (Supplementary Table 1).

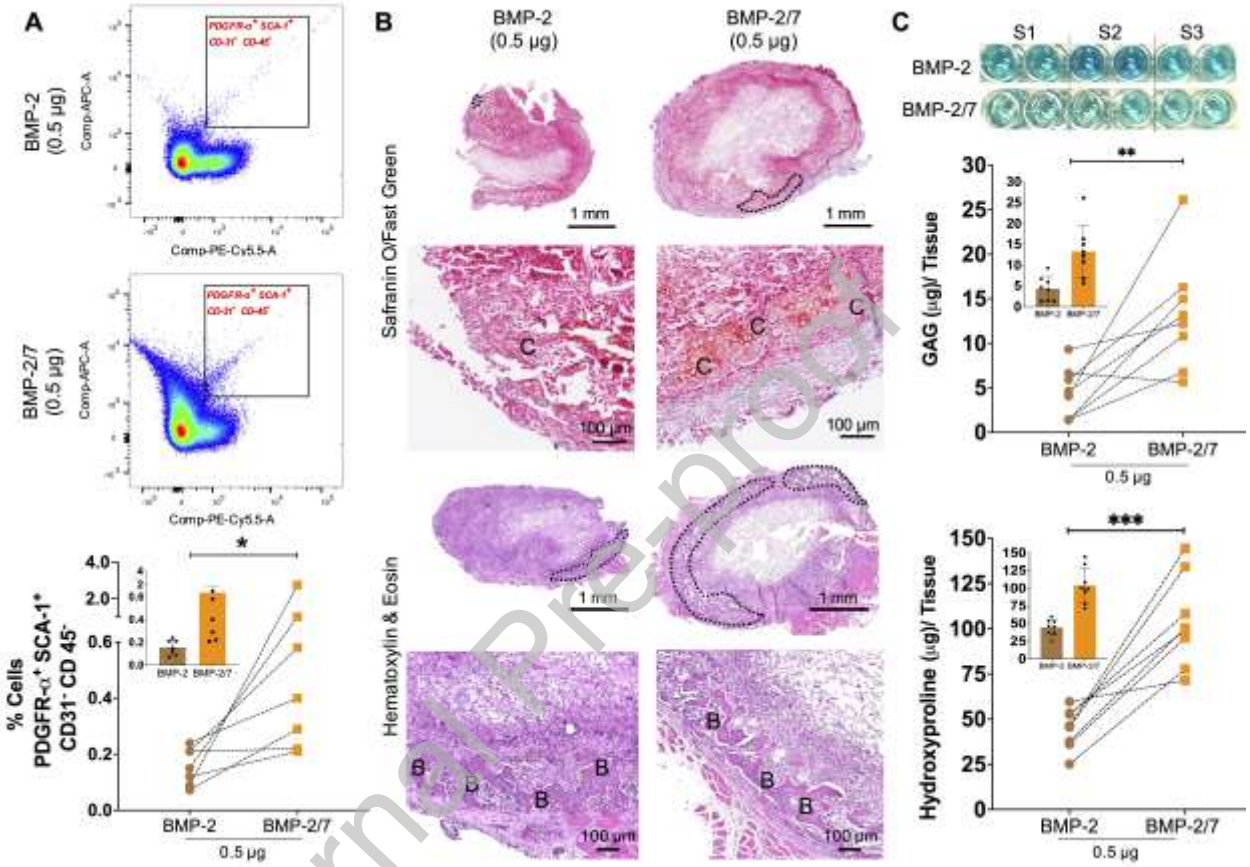

Figure 3: Cellular, histological, and biochemical characterization of the neo-tissue formed after 10-days of BMP-2 (0.5 µg) or BMP-2/7 (0.5 µg) treated CHA scaffold implantation in the abdominal muscle pouch of rats performed in a biologically paired experimental setup. (A) Flow cytometry based characterization of progenitor cell homing in the BMP-2 (top) and BMP-2/7 (middle) treated CHA scaffolds (n=7). The representative scatter plots and the gating indicates PDGFR-α^+, SCA-1^+, CD-31^-, and CD-45^- progenitor cell homing in the respective growth factor treated scaffold. Bottom panel in A indicates a pairwise comparison of the % of progenitor cells (out of total cells analyzed) homed in BMP-2 vs. BMP-2/7 treated CHA scaffolds. Inset in A, bottom represents mean ± SD of the same data. (B) Histological characterization of the neo-tissue formed after implanting CHA+BMP-2 or CHA+-BMP-2/7 treated scaffolds using

Safranin O/Fast green (top) and hematoxylin and eosin (bottom) (n=2). In the histology images, C indicates tissue regions with chondrocytes; B indicates regions with bone matrix; dashed black indicates regions with prominent cartilage (top) and bone (bottom) tissue. (C) Biochemical characterization of the neo-tissue matrix using Alcian blue assay for colorimetric glycosaminoglycan (GAG) quantification: top indicates 3 representative samples from each group; middle: total GAG/tissue) (n=8); bottom: hydroxyproline assay for collagen quantification (n=8). Data in the main panels is represented pairwise while inset represents mean ± SD. *, **, and *** indicates $p<0.05$, $p<0.01$, and $p<0.001$, respectively and actual p-values are presented in Table S5.

Transcriptomic signature of BMP-2/7 loaded CHA scaffolds elucidates upregulation of key genetic determinants of bone formation

In comparison with the pristine non-BMP loaded CHA scaffolds, a total of 691 genes were found to be commonly regulated in BMP-2/7 and BMP-2 treated CHA scaffolds; 1069 were specific to BMP-2/7, and 257 were specific to BMP-2 (Fig. 4A, B cut-off absolute fold change>2 and $p<0.05$). In an unbiased analysis of the 15 most differentially expressed genes, a majority of the genes were associated with cartilage development, morphology and size of bone and bone mineralization, most notable of which were *Ibsp, Panx3, Dmp1, Satb2, Cdh2, Dlx5, Mmp13, Vdr, Pth1r, Sp7, Runx2* and *Alpl* (Fig. 4C-E, supplementary table 2, and 3) and these genes were more highly expressed with BMP-2/7 treatments. Finally, when performing a direct comparison of BMP-2/7 and BMP-2 treated CHA scaffolds/regenerated neo-tissue specimens, BMP-2/7 showed significant upregulation of genes responsible for bone formation (*Bglap*, *Vdr*, *Pth1r,* and *Alpl*), BMP signalling (*Dlx5*, *Ccn1*, *Bmp4,* and *Bmp6*) and endochondral ossification (*Mmp13*, *Dmp1*, *Ccn1,* and *Sik3*) (Fig. 4F, G, supplementary tables 2, and 3).

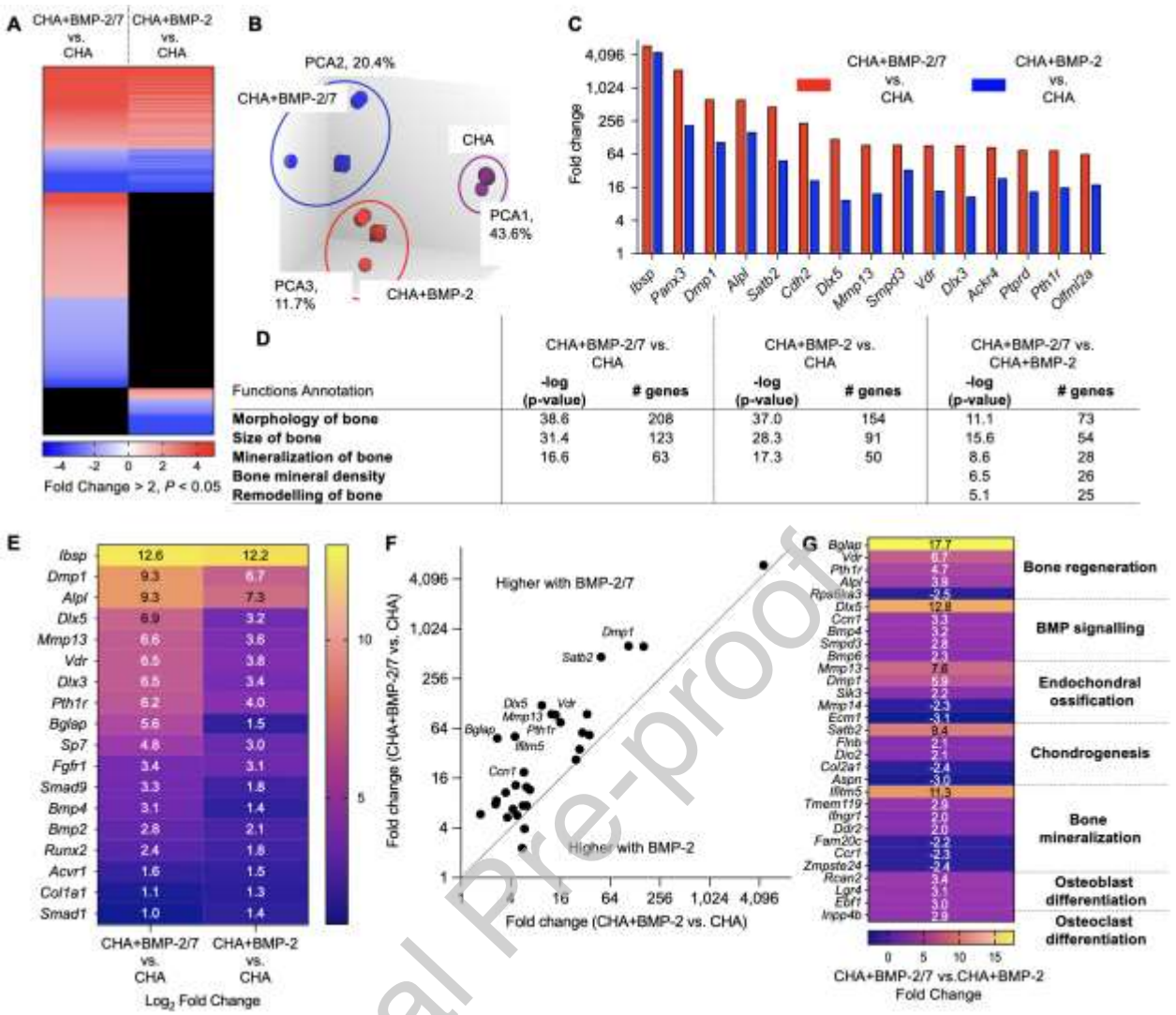

Figure 4: Transcriptomic signature of the neo tissue constructs formed after 10-days of implantation with CHA scaffold loaded with or without BMP-2 (0.5 μg) and BMP-2/7 (0.5 μg). (A) Heat map of all genes found to be common and specifically expressed in BMP-2/7 and BMP-2 treated scaffolds compared with pristine CHA scaffolds without the addition of any growth factor (n=3). (B) PCA plot indicating the % of most differentially expressed genes in each treatment group. (C) Bar graph of 15 most differentially expressed genes in BMP-2/7 and BMP-2 treated scaffolds in comparison with CHA scaffolds. (D) Most significantly regulated functions in CHA+BMP-2/7 vs. CHA (left), CHA+BMP-2 vs. CHA (middle) and CHA+BMP-2/7 vs CHA+BMP-2 (right) shows a strong regulation of bone-related functions in the BMP treated scaffolds. (E) A heat map of differentially expressed genes on the Log_2 scale indicating the log scale induction of conventional genetic markers associated with bone regeneration. (F) Comparison of genes upregulated with BMP-2/7 as well as BMP-2 treatment with respect to pristine

CHA scaffolds. (G) List of key genes associated with bone regeneration, BMP signaling, endochondral ossification and bone mineralization and their fold-change expression presented after a direct comparison of BMP-2/7 vs. BMP-2 treatment.

BMP-2/7 and BMP-2 release kinetics from the CHA scaffold indicates a similar sustained release profile for both proteins

To establish that the increased osteoinductivity of BMP-2/7 was not associated with the release pattern of the protein from the CHA scaffold, we studied the in-vitro and in-vivo release kinetics of both proteins using well established methods [15, 38, 39]. In-vitro release kinetics experiment indicated an early burst release of approximately 5% (100 ng/mL) for both BMP-2/7 and BMP-2 during the first 24 h (Fig. 5A, B). At later time points, the proteins were released at a more sustained pace and approximately 10% of the loaded protein was released over the 5-week period. On the contrary, the ACS scaffold demonstrated an increased release of both BMP-2 and BMP-2/7 at all time points when compared with the CHA scaffold and nearly 60% of the total loaded protein was released in 5-weeks. No differences in the in-vitro release kinetics could be observed for both the proteins for both ACS and CHA materials at any of the time points.

To determine the in-vivo pharmacokinetics of BMP-2/7 and BMP-2, in-vivo imaging (IVIS) was performed on mice implanted with fluorescently labelled protein loaded CHA scaffolds in the subcutaneous space on the dorsum. In-vivo release kinetics data demonstrated a progressive deterioration in the fluorescence signal with the passage of time (Fig. 5C). Importantly however, both proteins were retained at the implantation site for up to 20 days, after which the signal-to-noise ratio was significant enough to impact robust quantification. The fluorescence image analysis from the IVIS experiment indicated a significant drop (~ 40%) in signal intensity between 2 h and 24 h time point,

corroborating well with the initial burst release of the protein. Beyond the 24 h time point, the signal gradually reduced at each time point until the end of the experiment on day 20, at which time the signal was reduced to 25% of the initial measurement at 2 h (Fig. 5D).

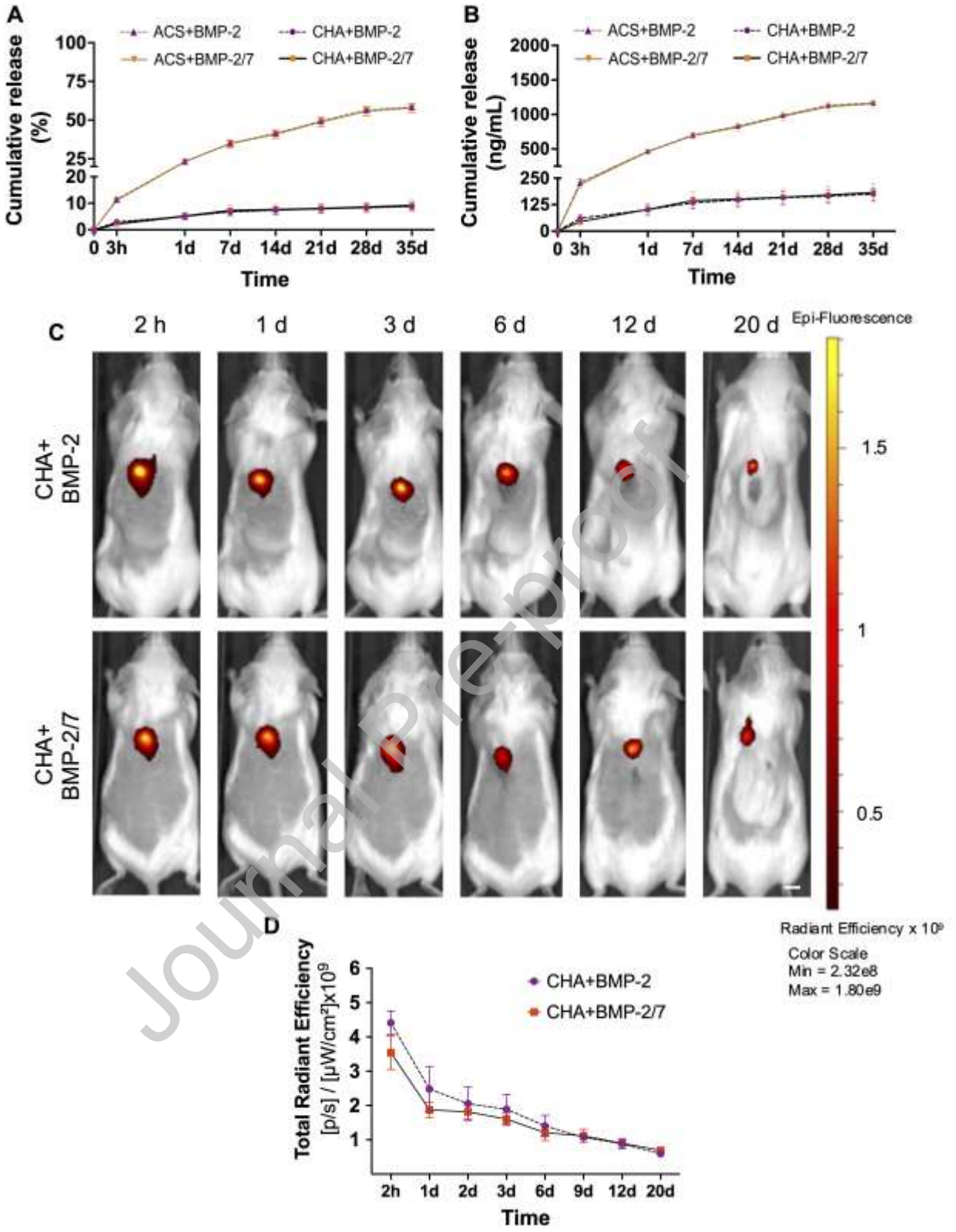

Figure 5: BMP-2 and BMP2/7 release kinetics. (A, B) Shows the in-vitro cumulative release in % (A) and in absolute values (concentration) (B) for BMP-2 and BMP-2/7 released from the CHA and ACS scaffolds; the data are presented as mean ± SD with n=5 for each protein and time point. (C) A mouse model (using BALB/c mice) of

subcutaneous implantation was used to study the in-vivo BMP-2 and BMP-2/7 release from the CHA scaffold, and the images represent one mouse from each treatment group at different time points. Implants were prepared using fluorescently labeled (VivoTag 680 NIR) BMP-2 or BMP-2/7 proteins. Labeled BMP-2 or BMP-2/7 loaded CHA scaffolds were deposited on the dorsum of mice. The mice were analyzed by longitudinal in-vivo fluorescence imaging using the IVIS spectrum. Representative images show fluorescence acquisition from mice at 2 h to 20 days after the implantation. (D) The bar graph shows the in-vivo release kinetics plotted as fluorescence measured from the region of interest (ROI) around the implantation site using the IVIS images; the data is presented as mean ± SD with 6 mice per treatment (n=12). Scale bar indicates ~3 mm.

Ultra-low dose BMP-2/7 delivered via a CHA scaffold promotes critical femoral defect healing in rats

Early response to BMP-2/7 treatment shows accelerated fracture healing in comparison with dose matched BMP-2

After establishing the increased potency of the BMP-2/7 delivered via the CHA scaffolds in the muscle pouch model and its release kinetics, we then tested the efficacy of the developed delivery system in a rat critical femoral defect model with the goal to reduce the overall BMP doses required for efficient healing [31]. BMP-2 (10 μg) delivered using the CHA scaffold was used as a positive control, since majority of previous studies have shown complete healing with this BMP-2 dose. The experimental dose of 0.5 μg was chosen based on the fact that the critical fracture healing with such low dose of BMP-2 has not been successful in earlier studies [20, 40] and we hypothesized that due to an increased osteoinductive effect, BMP-2/7 could potentially be sufficient at this dose. At 3-weeks, PET-CT imaging with Na-^{18}F revealed minimal tracer uptake in the defect gap in the empty and the CHA scaffold group (Fig. 6A). Growth factor loading of the CHA scaffolds with either BMP types enhanced the radioactive tracer uptake irrespective of the dose (Fig. 6A, bottom).

At 4-weeks, none of the specimens in the empty, CHA and BMP-2 (0.5 μg) group were radiographically bridged while 10 out of 12 specimens bridged in the BMP-2 (10 μg) group. Quite remarkably, 9 out of 13 specimens achieved radiographic bridging (Fig. 6B, top left) in the BMP-2/7 (0.5 μg) group already at the 4-week time point, showing significantly better results than a dose-matched BMP-2 group. When compared with BMP-2 (0.5 μg), the BMP-2 (10 μg) and BMP-2/7 (0.5 μg) groups exhibited significantly higher radiographic union scale scores (modified RUST; a marker for radiographic healing adapted for femur fractures) (Fig. 6B, bottom left). Micro-CT based 3D reconstructions indicated complete defect regeneration only in CHA scaffolds loaded with BMP-2 (10 μg) and BMP-2/7 (0.5 μg) with continuous cortices across the entire length of the defect (Fig. 6C, top right). Quantification of bone volume in the defect ROI indicated significantly higher BV in the BMP-2 (10 μg) and BMP-2/7 (0.5 μg) treated groups when compared with BMP-2 (0.5 μg) group (Fig. 6C, bottom right). At the intermediate time points of 6 and 8 weeks, BMP-2/7 (0.5 μg) group performed at par with BMP-2 (10 μg) group in terms of radiographic healing and RUST score (Supplementary Figure 8). However, it is important to note that the micro-CT based BV was significantly higher in the BMP-2 (0.5 μg) group when compared to BMP-2/7 (0.5 μg) group ($p<0.05$).

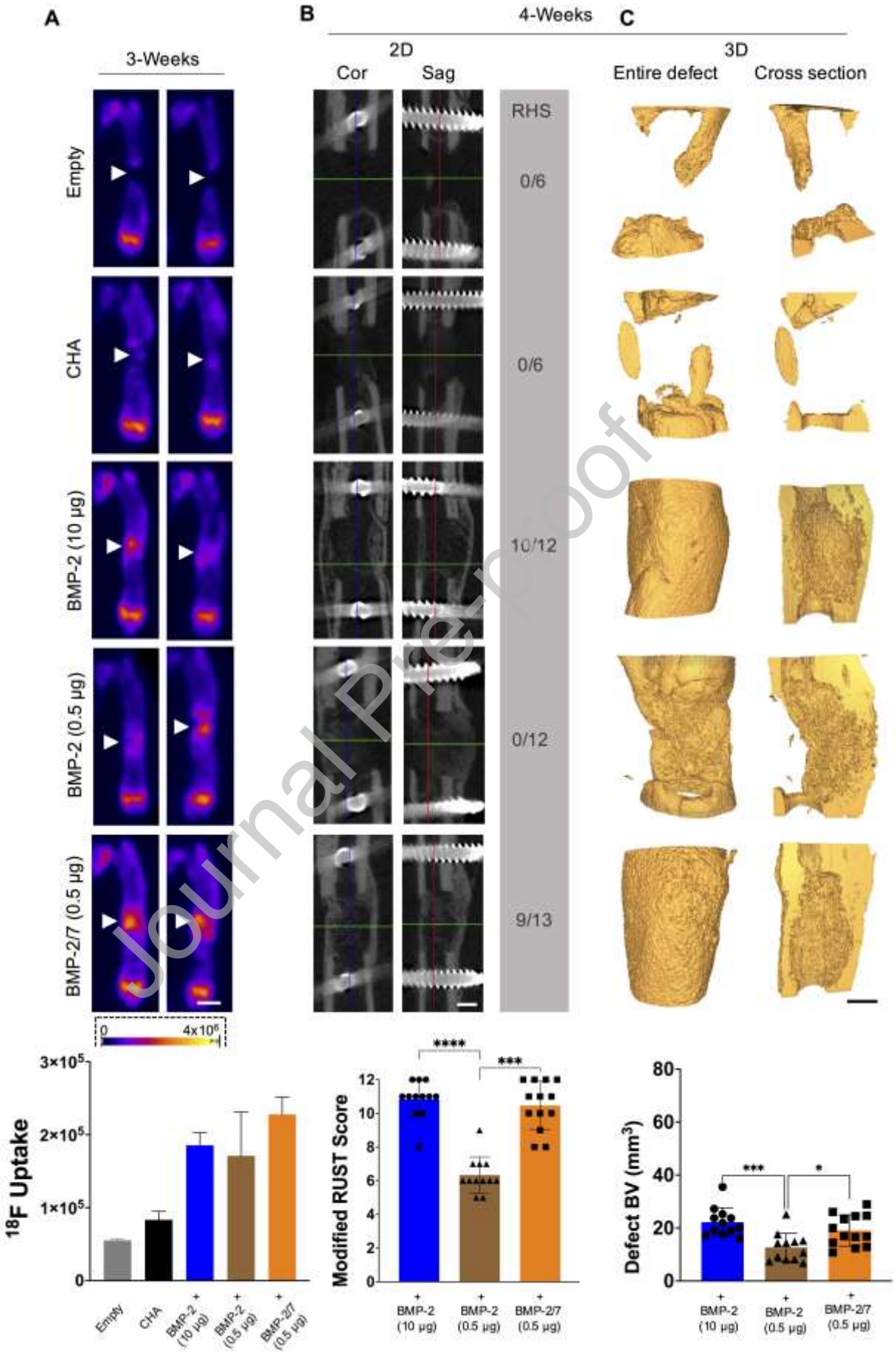

Figure 6: Fracture healing at 3- and 4-weeks using BMP-2 and BMP-2/7 loaded CHA scaffolds. (A) Shows two representative images from each group obtained during the PET-CT imaging using a bone seeking tracer ^{18}F with the arrow heads pointing to the tracer uptake in the defect gap. The scatter bar graph in the bottom shows the quantitative uptake of the ^{18}F tracer in a defined region of interest (ROI) in the fracture gap (n=2 for empty group and n=3 for the rest of the groups). (B, left) In-vivo micro-CT based representative 2D coronal and sagittal views from the middle of the defect along with the total number of defects bridged in each treatment group at 4-weeks. The bar graph in the bottom indicates the results from the modified radiographic union scale (RUST) scoring. (B, right) Representative 3D images of the entire defect area and some native bone in both whole and cross-sectional views and the bar graph in the bottom indicates quantification of micro-CT based bone volume (BV) in the defect (ROI height=4.5 mm). In panels B and C, n=6 for empty and CHA groups, n=12 for BMP-2 (10 μg) group and BMP-2 (0.5 μg) group and n=13 for BMP-2/7 (0.5 μg) group. Data in the bar graphs is presented as mean±SD. Scale bar in A represents ~5 mm, B represents ~1.5 mm and C represents ~2 mm. *, *** and, **** indicates $p<0.05$, 0.001, and 0.0001, respectively. Actual p-values are presented in Table S5.

BMP-2/7 loading of CHA scaffolds perform similar to a 20-times higher dose of BMP-2: Comparison of defect healing at the terminal time point of 12-weeks

At the terminal time point of 12-weeks, the empty and the CHA groups failed to bridge the bone defect (Fig. 7A-D, Supplementary Figures 9, 10, 11 and 15) confirming the critical size of the defect. Radiographically, both the positive control (BMP-2, 10 μg) group, and the BMP-2/7 (0.5 μg) group demonstrated exceptional radiographic outcome and achieved radiographic union in 10 out of 11 and 12 out of 13 specimens, respectively (Fig. 7A, Supplementary Figures 13-15). Conversely, only 7 out of 12 BMP-2 (0.5 μg) treated specimens had a completely bridged defect (Fig. 7A, Supplementary Figure 12 and 15). Other specimens failed to unite on at least two of the cortices, most often towards the side that was closer to the fixation plate. Furthermore, while the BMP-2 (10 μg) and BMP-2/7 (0.5 μg) specimens had a well-defined marrow cavity indicating

active bone remodelling, the marrow cavity in the BMP-2 (0.5 μg) specimens appeared to be different and was filled with cancellous bone like structures, most likely compensating for the unhealed cortices (Fig. 7A). BMP-2 (10 μg) and BMP-2/7 (0.5 μg) had higher RUST scores compared to BMP-2 (0.5 μg) (Fig. 7A, bottom). Despite a significantly better RUST score in the BMP-2 (10 μg) and BMP-2/7 (0.5 μg) groups, no differences in the bone volume was observed for BMP-2 (10 μg) vs. BMP-2/7 (0.5 μg), while the bone volume in the BMP-2 (0.5 μg) was significantly higher than the BMP-2/7 (0.5 μg) group (Fig. 7B, bottom). This was most likely caused by the excessive intra-medullary bone formation in the BMP-2 (0.5 μg) group.

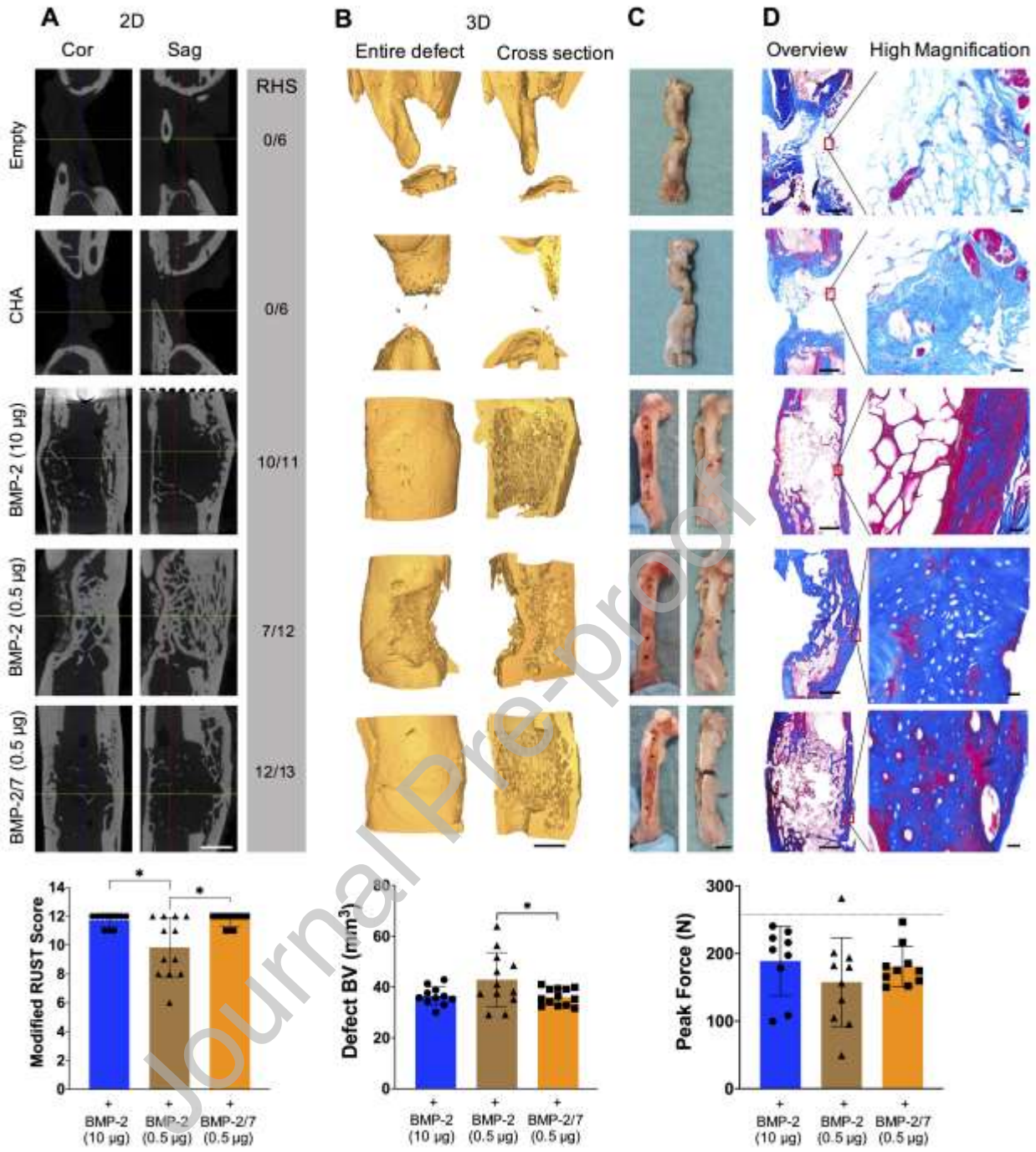

Figure 7: Fracture healing at 12 weeks using BMP-2 and BMP-2/7 loaded CHA scaffolds. (A) Ex-vivo micro-CT based representative 2D coronal and sagittal views from the middle of the defect along with the total number of defects bridged in each treatment group at 12-weeks. The bar graph in the bottom indicates the results from the modified radiographic union scale (RUST) scoring. (B) Representative 3D images of the entire defect area and some native bone in both whole and cross-sectional views and the bar graph in the bottom indicates quantification of micro-CT based bone volume (BV) in the defect (region of interest height=4.5 mm). (C) Digital photographs of specimens taken at

the time of harvest, and images post 3-point bending test (i.e. only for BMP treated groups, right panel). The bar graph in the bottom shows the peak force required to fracture specimens from different treatment groups. Dashed black line in panel C indicates the average peak force to fracture the contralateral femurs. (D, left) An overview image of the histologically stained specimens (Masson's trichrome); notice that only BMP-2 (10 μg) and BMP-2/7 (0.5 μg) specimens show completely bridged cortices, also shown by the micro-CT images (panels A, B). (D, right) High magnification images selected to emphasize the tissue composition in the area of the original defect. In bottom panels of A and B, n=6 for empty and CHA groups, n=11 for BMP-2 (10 μg) group, n=12 for BMP-2 (0.5 μg) group and n=13 for BMP-2/7 (0.5 μg) group and. In bottom panel of C, n=9 for BMP-2 (10 μg) group, n=10 for BMP-2 (0.5 μg) and BMP-2/7 (0.5 μg) groups. Scale bar in A represents ~2 mm, B represents ~2 mm, and C represents ~5 mm. Scale bar in the overview images in D represents ~1.5 mm, and high magnification images represents 0.1 mm. * indicates $p<0.05$. Actual p-values are presented in Table S5.

In terms of mechanical healing of the fractures, no apparent differences in the peak fracture force could be observed between any of the BMP treated groups (Fig. 7C, bottom). Similar results were observed for other flexural parameters including stiffness and work to fracture (Supplementary Figure 16). Furthermore, complete restoration of mechanical properties (with respect to the non-fractured contralateral femur) could not be observed for any of the BMP treated groups (Supplementary Figure 17). Micro-CT based quantification of the bone mineral density (BMD) of the regenerated bone in the defect region indicated that the BMD in the defect area was significantly lower than the BMD of a similar region in the contralateral femur in all treatment groups (Supplementary Figure 18). This lack of hydroxyapatite maturation could possibly be responsible for the results concerning the strength restoration of the regenerated bone. Similar results were also observed for cortical bone volume in the defect region in all treatment groups (Supplementary Figure 19).

Histology results corroborated well with the radiographic and micro-CT analysis. As it can be seen in the representative images in Fig. 7D, both BMP-2 (10 μg) and BMP-2/7 (0.5 μg) groups, demonstrated that the defect gap was filled with cortical bone along the entire length of the defect (Fig. 7D). Further, the intramedullary canal was filled with bone marrow like tissue. BMP-2 (0.5 μg) group demonstrated cortical bridging on only one side, while the side with the PEEK fixation plate failed to show cortical bridging. The intramedullary space in the BMP-2 (0.5 μg) groups was filled with unorganized cancellous structures as also seen in the micro-CT images. The defect gap in the empty and the CHA alone groups was predominantly filled with fibrous tissue or no tissue at all.

Discussion

Orchestrating bone regeneration is a complex undertaking due to the involvement of multiple cell types and signaling molecules. Yet, some BMP family proteins can drive the entire process unaided, right from initiating cell migration/homing to bone remodeling [41]. Despite all the promising pre-clinical/clinical data and widespread use, BMP-2 has also garnered criticism, particularly from its clinical users [14]. Exorbitant therapeutic doses and an inefficient delivery system comprising of a type I collagen sponge are often cited as the culprits for the decline in the usage of BMP-2 in the clinical settings [14]. To overcome the current challenges associated with sub-optimal BMP delivery systems and the use of supraphysiological doses, significant research has been carried out towards developing novel carrier systems that can be tailored to provide a sustained protein release. In parallel, considerable amount of research has also gone into evaluating other BMP family proteins and genes and designing cell-free extra cellular matrix (ECM) templates in the quest for using physiological growth factor doses in experimental fracture healing [15, 31, 42-44]. Herein, we aimed to combine the above

mentioned two approaches to create an off-the-shelf substitute for long bone reconstruction in a critical bone defect model in rats, hypothesized to recapitulate considerable bone trauma in the clinical situation [45].

We report that a heterodimer of BMP-2/7 delivered via a CHA scaffold at near physiological doses is more osteoinductive than its commercially approved and clinically used counterpart BMP-2 homodimer. An in-vivo snapshot of the early stages involved in the bone “autoinduction” process indicated that the heterodimer significantly improves homing of osteoprogenitor cells at the implantation site, which consequently express upregulated levels of key genetic determinants of bone formation and enhanced cartilage and bone ECM components. We further show that an ultra-low dose of BMP-2/7 delivered via a CHA scaffold accelerated fracture healing in a critical femoral defect in rats, and that a 20-times higher dose of the homodimer BMP-2 was required to achieve a similar effect.

The rat muscle pouch model provides an excellent environment to test the osteoinductive properties of biomaterials alone or enhanced with growth factors. The muscle being the closest neighbor to bone nevertheless possesses a genuine lack of endogenous bone inducing signaling molecules, unless stimulated by inflammation, growth factors or genetic abnormalities [46], and the absence of a bone marrow niche. Irrespective of the low BMP-2/7 doses of 0.2 and 2 µg delivered using the CHA scaffold, significantly higher new bone formation was observed in the muscle pouch compared with respective BMP-2 doses. Various BMP-2 carrier systems have been evaluated in the rat muscle pouch model with variable degrees of success yet none of the previous studies have indicated osteoinduction at a 0.2 µg dose in this model. This not only

highlights the increased bone forming potential of BMP-2/7 but also the importance of sustained growth factor release kinetics from the CHA scaffolding system. Different in-vitro molecular mechanisms have been proposed to be responsible for the increased osteoinductivity of BMP-2/7. It has been shown using a zebrafish embryo model that the heterodimer of BMP-2/7, unlike homodimers of BMP-2 or BMP-7, possessed a strong affinity to the BMP receptors and a different receptor binding-mechanism leading to an efficient activation of downstream signaling [47-49]. Zhu and co-workers have also shown that Noggin, the BMP antagonist does not effectively block the activity of the heterodimer leading to an improved osteoinductive effect compared to the respective BMP-2 and 7 homodimers [50]. Another similar attempt to decipher the improved bioactivity of BMP-2/7 by Miao et al. showed that BMP-2/7 mediated downstream signaling is not only dependent on the canonical Smad pathway but also an appreciable upregulation of the extracellular signal-related kinase (ERK) [17]. Here, for the first time, we report the in-vivo effects of prolonged BMP-2/7 delivery on progenitor cell homing, neo-tissue characteristics and fracture healing on a sophisticated mechanistic level.

After establishing the increased osteoinductive effect of BMP-2/7, we first aimed to compare progenitor cell homing capabilities of both BMP-2/7 and BMP-2 at an early time point of 10 days. The timepoint was chosen based on previous experiments, and the time interval between 1-2 weeks represents the post inflammatory reparative/regenerative phase where both cartilage and bone induction has been observed in rodents [51, 52]. Earlier studies have indicated that platelet derived growth factor receptor-α^+ (PDGFR-α^+) cells are resident in the interstitial tissue in the muscle and are responsible for heterotrophic ossification [37, 53]. Interestingly, Morikawa and co-workers [36] demonstrated that PDGFR-α and SCA-1 could be used for isolation of a

potent MSC sub-type of non-hematopoietic origin (CD-45$^-$, CD-31$^-$) found in the endosteal linings of long bones [54]. Taken together, these findings strongly suggest that PDGFR-α$^+$, SCA-1$^+$, CD-45$^-$, and CD-31$^-$ cells forms an important progenitor cell population in bone regeneration. Quite evidently, BMP-2/7 led to a significantly increased homing of progenitor cells in the CHA scaffold/neo-tissue construct compared to BMP-2 loaded CHA implant in our model, which could potentially be responsible for imparting BMP-2/7 with superior osteoinductive properties. To further characterize the biochemical and genetic signature of the neo-tissue at an early stage of regeneration, evaluation of matrix composition and microarray analysis was performed. It was confirmed that the neo-tissue formed after BMP-2/7 loaded CHA scaffold implantation contained significantly more total GAG and collagen. These are key components of cartilage and bone ECM and are upregulated during endochondral ossification [55]. The use of BMP-2/7 also led to a significant upregulation of *Mmp13 and Dmp1*, key genes upregulated during endochondral ossification [56-58], *Dlx5*, a BMP responsive translational activator responsible for osteoblast differentiation [57, 58] as well as the classical genetic determinants of bone formation such as *Bglap, Alp, Pth1r* and *Vdr*.

To ascertain that the differences in the osteoinductive potential of the two BMP molecules tested in this study did not emanate from the differences in the release kinetics of the respective proteins from the CHA scaffold, we tested both in-vitro and in-vivo release kinetics of the two molecules. Both in-vitro and in-vivo data indicated an initial burst release followed by a more prolonged release at least for 3-weeks. Carrier systems for BMP-2 delivery comprise of polymers, ceramics or composites with tunable release characteristics [59], but due to the excellent biocompatibility and biochemical resemblance to bone ECM, collagen based delivery systems were first to be clinically

approved. Experimental studies on the pharmacokinetics of BMP-2 loaded collagen sponges have shown a very rapid “early” burst release of up to 30% within the first 3 hours of implantation, 50% within 3 days and a complete release in a period of less than 2-weeks [16]. Jeon et al. and La et al. emphasized the importance of tailoring the BMP-2 release by comparing bone formation at ectopic and orthotopic locations, respectively using a rapid release system (mimicking BMP-2 release kinetics from the absorbable collagen sponge (ACS) scaffold) and a slow release delivery system [60, 61]. They convincingly demonstrated that a more gradual release of recombinant human BMP-2 was required for better bone regeneration in both models. Considering the results from the in-vitro protein release assay in this study, much of the BMPs are actually retained in the CHA scaffold contrary to the ACS scaffold and this difference in release (ACS) vs. retention (CHA) might explain the superiority of the CHA scaffold as a BMP delivery system. BMP-2 has been shown to have a short biological half-life of a few minutes [62], which implies that the protein has a very short time to bind to its target and failure to do so would render the protein ineffective. Contrary to the in-vitro protein release assay, the in-vivo release of BMPs from the CHA scaffold was higher and this is in line with previous reports [15, 63]. The in-vivo environment is more dynamic and the biomaterial is continually exposed to proteases and cells that can mediate a faster degradation of the material and thereby lead to an increased protein release. Based on the results from this study as well as the previous reports, we therefore recommend that BMP delivery systems be characterized in both in-vitro and in-vivo assays in order to establish the efficacy of the delivery system.

Collagen and hydroxyapatite not only mimic the organic and inorganic components of bone but recently Lackington and co-workers showed that by incorporating

hydroxyapatite in the collagen scaffolds, more prolonged release of BMP-2 could be achieved [23]. In fact, it was hydroxyapatite Urist and co-workers used in the purification of BMP in their very early protocols [64]. BMP-2 interaction with HA is electrostatically controlled via the formation of water bridged hydrogen bonds with the hydroxyl, amine and carboxylic domains interacting individually or in tandem with the HA crystal depending on the protein orientation [65]. Despite a short BMP incubation time of 10 min, significantly more BMP was retained in the CHA scaffolds when compared to the ACS biomaterial. Our results from the BMP-HA interaction are in line with the previous findings and provide a mechanistic insight into BMP-HA binding, which makes CHA scaffolds superior to the FDA-approved ACS material. Many strategies for successfully customizing BMP release using techniques such as nano/micro particle based carriers or functionalized polymer/ECM scaffolds have been devised [59, 66-69]. However, the degree of complexity involved in the fabrication and upscaling of such systems is cumbersome and face challenging regulatory hurdles leading to slow clinical translation.

Following the studies involving the release kinetics of the two BMP molecules from the CHA scaffold, we then investigated the role of BMP-2/7 in fracture healing. The results from the femur defect study showed that 0.5 µg BMP-2/7 loaded CHA scaffolds accelerated radiographic union rate already at 4-6 weeks, which was at par with high dose BMP-2 (10 µg) loaded CHA scaffolds. The accelerated bone forming potential of BMP-2/7 was verified early on at 3-weeks using Na-^{18}F, a marker of bone formation which preferentially binds to exposed hydroxyapatite particles laid out by the osteoblasts in the new bone matrix. Mathavan and co-workers have shown that increased uptake of this tracer at an early time point provides a good prognostic tool for the early detection of bony union [51]. In-vivo radiology and micro-CT data corroborated well with the initial

PET-CT findings. Mechanical testing of the “mechanically” consolidated femurs at the terminal time point did not show any differences in peak force between different BMP treated groups and neither did any of the groups show complete restoration of mechanical properties at the terminal time point of 12-weeks. The use of the rigid fixation setup in our study could be a potential confounding factor responsible for delaying the physiological bone remodeling and consequent mechanical properties. Previous fracture healing studies have demonstrated that the use of stiff fixation plates can have a negative effect on the mechanical properties of healing fractures in similar animal models [70], and the use of compliant fixation methods that allow for dynamic in-vivo loading during fracture healing could be evaluated in future studies [71-73]. These hypotheses are supported by the data on BMD as well as cortical bone volume, both of which show that despite successful cortical bridging in many of the specimens, the BMD and the cortical BV was not restored completely in comparison with the healthy contralateral side. Histology corroborated well with the micro-CT findings and showed the presence of fully bridged cortices as well as a well-defined intramedullary space in both BMP-2/7 and BMP-2 (10 µg) groups. These results are of clinical importance and show that an ultra-low dose of BMP-2/7 not only reduces the overall healing time, but the healing is at par with high dose BMP-2. Early fracture healing has direct implications on both load bearing, which has been shown to be a key factor in long bone fracture healing [74] as well as in reducing fracture associated costs, both for the patient and the public healthcare system. Caution must however be taken with the use of BMP-2/7 in clinical use especially since it is an experimental molecule, unapproved by the healthcare regulatory agencies. In addition, future studies on large animal models must be performed before clinical translation.

The FDA approved dosage for the use of BMP-2 in tibial shaft fractures is 1.5 µg/mm^3 of the ACS carrier material [75], although even higher doses have been reported in off-label studies [76]. In our study, we used a scaffold volume of approximately 63 mm^3 to deliver 0.5 µg of the heterodimer BMP-2/7, which led to a radiographic union in 12 out of 13 tested animals. The used BMP-2/7 dose in this study equates to a dose of 0.008 µg/mm^3, or an overall dose reduction by 187 times, which is a significant step towards the use of physiological growth factor doses in fracture healing. On the contrary, it was demonstrated that a 0.16 µg/mm^3 dose of the homodimer BMP-2 was required to achieve similar results, once again highlighting the potency of BMP-2/7 in an orthotopic environment. Despite a 20-fold difference in the doses of BMP-2 and BMP-2/7 required to achieve radiographic healing, it is important to highlight that even the BMP-2 dose used in this study was approximately 10 times lower than the recommended dose of 1.5 µg/mm^3, used with the ACS biomaterial. In an earlier study involving the delivery of 0.4 µg BMP-2/7 via a collagen sponge in a similar animal model, Zhang et al., demonstrated inconsistent bridging of the bone defects and ectopic bone formation in all treated specimens [20]. This difference again highlights and verifies the importance of incorporating hydroxyapatite in bone targeted drug delivery devices required for achieving a controlled and sustained spatial growth factor release kinetics [77-80]. Ectopic bone formation is another important matter of concern with the use of BMP-2 especially when used in areas of proximity to major nerves, such as during spinal indications [81]. Irrespective of the type and dose of BMP used in our study, we did not observe any ectopic bone formation in the femur defect model during the entire course of observation. Reduction of therapeutic BMP doses is of clinical importance and we have shown that by providing a sustained release of the more potent BMP-2/7 molecule

using the CHA scaffold delivery system, it is possible to reduce the side-effects associated with the use of BMP-2.

Although the use of BMP-2/7 delivered via the CHA scaffolds shows promising results in our work so far, it is important to acknowledge some of the limitations of this study. Despite accelerated radiographic fracture healing in BMP-2/7 treated animals, the mechanical properties of the regenerated tissues were evaluated only at the terminal time point at which all BMP treated specimens had similar mechanical properties. We believe that the information on dynamic changes in the mechanical properties of the regenerated bone over the entire course of healing as well as data on complete restoration of mechanical properties are missing in this study. Future studies would require focusing on answering these important questions, perhaps by studying the change in mechanical properties of bone over time or by using dynamic in-vivo loading during the course of fracture healing and by extending the study duration to later time points. It is also noteworthy to mention that the specimens that demonstrated cortical bridging early on maintained the cortical structure throughout the course of the experiment while similar was true for the specimens that demonstrated woven bone morphology. Understanding the factors causing these differences in bone architecture could be an important future step in order to improve the overall union rates. Although, 0.5 μg dose BMP-2/7 was sufficient for fracture healing in this model, both time and minimum BMP-2/7 doses required for complete radiographic and mechanical healing need to be further identified as the most important challenge in BMP mediated bone regeneration is to use the least amount of growth factor doses in order to avoid side effects. Finally, BMP-2/7 heterodimer was only compared with homodimer BMP-2 and not BMP-7. In light of the existing data, BMP-7, in general is less potent than BMP-2 [20,

82] and earlier studies have already compared the two homodimers to the heterodimer BMP-2/7 and concluded that BMP-2/7 is more potent than the respective homodimers [17]. From a clinical perspective, BMP-7 has been discontinued from the market making its evaluation in this study less relevant from a translational perspective.

Conclusion

In this study, we show that the presence of hydroxyapatite in CHA scaffolds allows for significantly improved sequestration and effective delivery of BMP when compared to a pristine collagen biomaterial. We then report that a heterodimer of BMP-2/7 delivered using a CHA scaffold possesses significantly better osteoinductive properties than the current FDA-approved growth factor BMP-2. At the molecular level, we found that BMP-2/7 treatment of CHA scaffolds in comparison to BMP-2 treated CHA scaffolds led to an increased chemotaxis of progenitor cells, which consequently presented with an upregulated transcriptomic signature favorable for bone regeneration. BMP-2/7 treatment led to formation of larger tissue in general and contained more cartilage and bone ECM components. We also show that the CHA scaffolding system provided a congenial release profile of both BMP-2 and BMP-2/7 for up to 5-weeks in-vitro and 3-weeks in-vivo and it was indeed the increased potency of the BMP-2/7 molecule that was responsible for the aforementioned effects rather than the difference in the release profile of the two molecules. Irrespective of the protein type, our results show that in terms of a sustained delivery system for BMP delivery, the protein release kinetics from the CHA scaffold with an initial BMP burst release followed by retention of the protein for 3-5 weeks appears to be critical to achieve optimal results. Finally, the use of an ultra-low dose BMP-2/7 aided in complete bridging of critical femoral defects in rats already at an early time point of 4-weeks, while a dose-matched BMP-2 molecule could only

achieve union in 7/12 specimens, even at the terminal time point of 12-weeks. A 20-times higher dose of BMP-2 was required to achieve results similar to BMP-2/7. This improved osteoinductive effect of BMP-2/7 is of significant clinical importance, especially to overcome the drawbacks associated with the use of high dose BMP-2. Combining the CHA scaffolds with a low dose BMP-2/7 could potentially be used as an off-the-shelf bone substitute in the future.

Author contribution

YL, EJS, SZ, FJOB, PEB, AS, DBR: Study design. EJS, FJOB: Scaffold preparation. YL, MP, JP, IA, SP, MWO, SS, CV, SZ, AS, PEB and DBR: Animal experimentation and data analysis. DBR and YL: First draft of the manuscript. All authors: Manuscript revision.

Author disclosures

DBR holds stocks in Moroxite AB and Moroxite F AB, which bears no conflict of interest with regards to this study. FJOB holds IP related to a scaffold of similar composition to that used in this study which is currently being commercialised by Locate Bio. All other authors have nothing to disclose.

Acknowledgements

DBR would like to thank the Maggie-Stephens Foundation (20202004), Sten K Johnsons Foundation (20210592) and the Crafoord Foundation (20210550) for the financial support required to conduct this research. We also thank the Lund University, Medical Faculty and the Lund University Bioimaging Center (LBIC) for the infrastructure support. FJOB acknowledges support by the by the Health Research Board (HRB) in Ireland

(grant number ILP-POR-2017-032), the EU BlueHuman Interreg Atlantic Area Project (EAPA_151/2016) and the European Research Council (grant agreement no. 788,753 - ReCaP).

Data Availability

All data pertaining to this manuscript has been presented in the main manuscript or the supplementary information. Raw data can be acquired from the corresponding author upon a reasonable request.

References

[1] J. Parvizi, G.K. Kim, Chapter 32 - Bone Grafting, in: J. Parvizi, G.K. Kim (Eds.), High Yield Orthopaedics, W.B. Saunders, Philadelphia, 2010, pp. 64-65.
[2] A. Kinaci, V. Neuhaus, D.C. Ring, Trends in bone graft use in the United States, Orthopedics 37(9) (2014) e783-8.
[3] G.L. Koons, M. Diba, A.G. Mikos, Materials design for bone-tissue engineering, Nature Reviews Materials 5(8) (2020) 584-603.
[4] A.R. Amini, C.T. Laurencin, S.P. Nukavarapu, Bone Tissue Engineering: Recent Advances and Challenges, 40(5) (2012) 363-408.
[5] A.R. Armiento, L.P. Hatt, G. Sanchez Rosenberg, K. Thompson, M.J. Stoddart, Functional Biomaterials for Bone Regeneration: A Lesson in Complex Biology, Advanced Functional Materials 30(44) (2020) 1909874.
[6] I. Martin, P.J. Simmons, D.F. Williams, Manufacturing Challenges in Regenerative Medicine, Science Translational Medicine 6(232) (2014) 232fs16-232fs16.
[7] H. Petite, V. Viateau, W. Bensaïd, A. Meunier, C. de Pollak, M. Bourguignon, K. Oudina, L. Sedel, G. Guillemin, Tissue-engineered bone regeneration, Nature Biotechnology 18(9) (2000) 959-963.
[8] E. Cenni, F. Perut, S.R. Baglío, E. Fiorentini, N. Baldini, Recent highlights on bone stem cells: a report from Bone Stem Cells 2009, and not only…, Journal of Cellular and Molecular Medicine 14(11) (2010) 2614-2621.
[9] M.B. Preda, C.A. Neculachi, I.M. Fenyo, A.-M. Vacaru, M.A. Publik, M. Simionescu, A. Burlacu, Short lifespan of syngeneic transplanted MSC is a consequence of in vivo apoptosis and immune cell recruitment in mice, Cell Death & Disease 12(6) (2021) 566.

[10] R.E. Guldberg, M.E. Oest, K. Dupont, A. Peister, E. Deutsch, Y. Kolambkar, D. Mooney, Biologic augmentation of polymer scaffolds for bone repair, J Musculoskelet Neuronal Interact 7(4) (2007) 333-4.
[11] A. Haumer, P.E. Bourgine, P. Occhetta, G. Born, R. Tasso, I. Martin, Delivery of cellular factors to regulate bone healing, Advanced Drug Delivery Reviews 129 (2018) 285-294.
[12] O.P. Gautschi, S.P. Frey, R. Zellweger, Bone morphogenetic proteins in clinical applications, ANZ J Surg 77(8) (2007) 626-31.
[13] S.N. Lissenberg-Thunnissen, D.J.J. de Gorter, C.F.M. Sier, I.B. Schipper, Use and efficacy of bone morphogenetic proteins in fracture healing, International Orthopaedics 35(9) (2011) 1271.
[14] A.W. James, G. LaChaud, J. Shen, G. Asatrian, V. Nguyen, X. Zhang, K. Ting, C. Soo, A Review of the Clinical Side Effects of Bone Morphogenetic Protein-2, Tissue Eng Part B Rev 22(4) (2016) 284-97.
[15] D.B. Raina, D. Larsson, F. Mrkonjic, H. Isaksson, A. Kumar, L. Lidgren, M. Tägil, Gelatin- hydroxyapatite- calcium sulphate based biomaterial for long term sustained delivery of bone morphogenic protein-2 and zoledronic acid for increased bone formation: In-vitro and in-vivo carrier properties, Journal of Controlled Release 272 (2018) 83-96.
[16] H. Uludag, D. D'Augusta, R. Palmer, G. Timony, J. Wozney, Characterization of rhBMP-2 pharmacokinetics implanted with biomaterial carriers in the rat ectopic model, J Biomed Mater Res 46(2) (1999) 193-202.
[17] C. Miao, D. Qin, P. Cao, P. Lu, Y. Xia, M. Li, M. Sun, W. Zhang, F. Yang, Y. Zhang, S. Tang, T. Liu, F. Liu, BMP2/7 heterodimer enhances osteogenic differentiation of rat BMSCs via ERK signaling compared with respective homodimers, J Cell Biochem (2018).
[18] T. Morimoto, T. Kaito, Y. Matsuo, T. Sugiura, M. Kashii, T. Makino, M. Iwasaki, H. Yoshikawa, The bone morphogenetic protein-2/7 heterodimer is a stronger inducer of bone regeneration than the individual homodimers in a rat spinal fusion model, Spine J 15(6) (2015) 1379-90.
[19] T. Kaito, T. Morimoto, Y. Mori, S. Kanayama, T. Makino, S. Takenaka, Y. Sakai, S. Otsuru, Y. Yoshioka, H. Yoshikawa, BMP-2/7 heterodimer strongly induces bone regeneration in the absence of increased soft tissue inflammation, The Spine Journal 18(1) (2018) 139-146.
[20] B. Zhang, J.D. Skelly, J.R. Maalouf, D.C. Ayers, J. Song, Multifunctional scaffolds for facile implantation, spontaneous fixation, and accelerated long bone regeneration in rodents, Science Translational Medicine 11(502) (2019) eaau7411.
[21] F.G. Lyons, J.P. Gleeson, S. Partap, K. Coghlan, F.J. O'Brien, Novel microhydroxyapatite particles in a collagen scaffold: a bioactive bone void filler?, Clin Orthop Relat Res 472(4) (2014) 1318-1328.
[22] J.P. Gleeson, N.A. Plunkett, F.J. O'Brien, Addition of hydroxyapatite improves stiffness, interconnectivity and osteogenic potential of a highly porous collagen-based scaffold for bone tissue regeneration, Eur Cell Mater 20 (2010) 218-30.
[23] W.A. Lackington, D. Gehweiler, I. Zderic, D. Nehrbass, S. Zeiter, A. González-Vázquez, F.J. O'Brien, M.J. Stoddart, K. Thompson, Incorporation of hydroxyapatite into collagen scaffolds enhances the therapeutic efficacy of rhBMP-2 in a weight-bearing femoral defect model, Materials Today Communications 29 (2021) 102933.
[24] E. Quinlan, E.M. Thompson, A. Matsiko, F.J. O'Brien, A. López-Noriega, Functionalization of a Collagen-Hydroxyapatite Scaffold with Osteostatin to Facilitate Enhanced Bone Regeneration, Adv Healthc Mater 4(17) (2015) 2649-56.

[25] E. Quinlan, E.M. Thompson, A. Matsiko, F.J. O'Brien, A. López-Noriega, Long-term controlled delivery of rhBMP-2 from collagen–hydroxyapatite scaffolds for superior bone tissue regeneration, Journal of Controlled Release 207 (2015) 112-119.
[26] D.B. Raina, H. Isaksson, W. Hettwer, A. Kumar, L. Lidgren, M. Tägil, A Biphasic Calcium Sulphate/Hydroxyapatite Carrier Containing Bone Morphogenic Protein-2 and Zoledronic Acid Generates Bone, Scientific Reports 6(1) (2016) 26033.
[27] T.L. Cheng, P. Valtchev, C.M. Murphy, L.C. Cantrill, F. Dehghani, D.G. Little, A. Schindeler, A sugar-based phase-transitioning delivery system for bone tissue engineering, Eur Cell Mater 26 (2013) 208-21; discussion 220-1.
[28] S. Björnsson, Simultaneous preparation and quantitation of proteoglycans by precipitation with alcian blue, Anal Biochem 210(2) (1993) 282-91.
[29] A. Struglics, S. Larsson, M.A. Pratta, S. Kumar, M.W. Lark, L.S. Lohmander, Human osteoarthritis synovial fluid and joint cartilage contain both aggrecanase- and matrix metalloproteinase-generated aggrecan fragments, Osteoarthritis Cartilage 14(2) (2006) 101-13.
[30] S. Larsson, L.S. Lohmander, A. Struglics, An ARGS-aggrecan assay for analysis in blood and synovial fluid, Osteoarthritis and Cartilage 22(2) (2014) 242-249.
[31] D.B. Raina, L.-M. Matuszewski, C. Vater, J. Bolte, H. Isaksson, L. Lidgren, M. Tägil, S. Zwingenberger, A facile one-stage treatment of critical bone defects using a calcium sulfate/hydroxyapatite biomaterial providing spatiotemporal delivery of bone morphogenic protein and zoledronic acid, Science Advances 6(48) (2020) eabc1779.
[32] J.M. Leow, N.D. Clement, T. Tawonsawatruk, C.J. Simpson, A.H. Simpson, The radiographic union scale in tibial (RUST) fractures: Reliability of the outcome measure at an independent centre, Bone Joint Res 5(4) (2016) 116-21.
[33] J. Sundermann, H. Zagst, J. Kuntsche, H. Wätzig, H. Bunjes, Bone Morphogenetic Protein 2 (BMP-2) Aggregates Can be Solubilized by Albumin—Investigation of BMP-2 Aggregation by Light Scattering and Electrophoresis, Pharmaceutics 12(12) (2020) 1143.
[34] M.R. Urist, Bone: formation by autoinduction, Science 150(3698) (1965) 893-9.
[35] D.D. Houlihan, Y. Mabuchi, S. Morikawa, K. Niibe, D. Araki, S. Suzuki, H. Okano, Y. Matsuzaki, Isolation of mouse mesenchymal stem cells on the basis of expression of Sca-1 and PDGFR-α, Nat Protoc 7(12) (2012) 2103-11.
[36] S. Morikawa, Y. Mabuchi, Y. Kubota, Y. Nagai, K. Niibe, E. Hiratsu, S. Suzuki, C. Miyauchi-Hara, N. Nagoshi, T. Sunabori, S. Shimmura, A. Miyawaki, T. Nakagawa, T. Suda, H. Okano, Y. Matsuzaki, Prospective identification, isolation, and systemic transplantation of multipotent mesenchymal stem cells in murine bone marrow, J Exp Med 206(11) (2009) 2483-96.
[37] T. Oishi, A. Uezumi, A. Kanaji, N. Yamamoto, A. Yamaguchi, H. Yamada, K. Tsuchida, Osteogenic differentiation capacity of human skeletal muscle-derived progenitor cells, PLoS One 8(2) (2013) e56641.
[38] A.-C. Strömdahl, L. Ignatowicz, G. Petruk, M. Butrym, S. Wasserstrom, A. Schmidtchen, M. Puthia, Peptide-coated polyurethane material reduces wound infection and inflammation, Acta Biomaterialia 128 (2021) 314-331.
[39] M. Puthia, M. Butrym, J. Petrlova, A.-C. Strömdahl, M.Å. Andersson, S. Kjellström, A. Schmidtchen, A dual-action peptide-containing hydrogel targets wound infection and inflammation, Science Translational Medicine 12(524) (2020) eaax6601.
[40] J.N. Zara, R.K. Siu, X. Zhang, J. Shen, R. Ngo, M. Lee, W. Li, M. Chiang, J. Chung, J. Kwak, B.M. Wu, K. Ting, C. Soo, High doses of bone morphogenetic protein 2 induce structurally abnormal bone and inflammation in vivo, Tissue Eng Part A 17(9-10) (2011) 1389-99.

[41] J.M. Wozney, V. Rosen, Bone morphogenetic protein and bone morphogenetic protein gene family in bone formation and repair, Clin Orthop Relat Res (346) (1998) 26-37.
[42] D.B. Raina, I. Qayoom, D. Larsson, M.H. Zheng, A. Kumar, H. Isaksson, L. Lidgren, M. Tägil, Guided tissue engineering for healing of cancellous and cortical bone using a combination of biomaterial based scaffolding and local bone active molecule delivery, Biomaterials 188 (2019) 38-49.
[43] S. Pigeot, T. Klein, F. Gullotta, S.J. Dupard, A. Garcia Garcia, A. García-García, S. Prithiviraj, P. Lorenzo, M. Filippi, C. Jaquiery, L. Kouba, M.A. Asnaghi, D.B. Raina, B. Dasen, H. Isaksson, P. Önnerfjord, M. Tägil, A. Bondanza, I. Martin, P.E. Bourgine, Manufacturing of Human Tissues as off-the-Shelf Grafts Programmed to Induce Regeneration, Advanced Materials 33(43) (2021) 2103737.
[44] L.D. Loozen, A. Vandersteen, A.H. Kragten, F.C. Öner, W.J. Dhert, M.C. Kruyt, J. Alblas, Bone formation by heterodimers through non-viral gene delivery of BMP-2/6 and BMP-2/7, Eur Cell Mater 35 (2018) 195-208.
[45] K. Sato, Y. Watanabe, N. Harada, S. Abe, T. Matsushita, K. Yamanaka, T. Kaneko, Y. Sakai, Establishment of reproducible, critical-sized, femoral segmental bone defects in rats, Tissue Eng Part C Methods 20(12) (2014) 1037-41.
[46] P.B. Yu, D.Y. Deng, C.S. Lai, C.C. Hong, G.D. Cuny, M.L. Bouxsein, D.W. Hong, P.M. McManus, T. Katagiri, C. Sachidanandan, N. Kamiya, T. Fukuda, Y. Mishina, R.T. Peterson, K.D. Bloch, BMP type I receptor inhibition reduces heterotopic [corrected] ossification, Nat Med 14(12) (2008) 1363-1369.
[47] S.C. Little, M.C. Mullins, Bone morphogenetic protein heterodimers assemble heteromeric type I receptor complexes to pattern the dorsoventral axis, Nat Cell Biol 11(5) (2009) 637-643.
[48] J. Christian, A tale of two receptors: Bmp heterodimers recruit two type I receptors but use the kinase activity of only one, Proceedings of the National Academy of Sciences 118(19) (2021) e2104745118.
[49] B. Tajer, J.A. Dutko, S.C. Little, M.C. Mullins, BMP heterodimers signal via distinct type I receptor class functions, Proceedings of the National Academy of Sciences 118(15) (2021) e2017952118.
[50] W. Zhu, J. Kim, C. Cheng, B.A. Rawlins, O. Boachie-Adjei, R.G. Crystal, C. Hidaka, Noggin regulation of bone morphogenetic protein (BMP) 2/7 heterodimer activity in vitro, Bone 39(1) (2006) 61-71.
[51] N. Mathavan, J. Koopman, D.B. Raina, A. Turkiewicz, M. Tägil, H. Isaksson, 18F-fluoride as a prognostic indicator of bone regeneration, Acta Biomaterialia 90 (2019) 403-411.
[52] K. Hashimoto, T. Kaito, M. Furuya, S. Seno, D. Okuzaki, J. Kikuta, H. Tsukazaki, H. Matsuda, H. Yoshikawa, M. Ishii, In vivo dynamic analysis of BMP-2-induced ectopic bone formation, Scientific Reports 10(1) (2020) 4751.
[53] M.N. Wosczyna, A.A. Biswas, C.A. Cogswell, D.J. Goldhamer, Multipotent progenitors resident in the skeletal muscle interstitium exhibit robust BMP-dependent osteogenic activity and mediate heterotopic ossification, J Bone Miner Res 27(5) (2012) 1004-17.
[54] D.D. Houlihan, Y. Mabuchi, S. Morikawa, K. Niibe, D. Araki, S. Suzuki, H. Okano, Y. Matsuzaki, Isolation of mouse mesenchymal stem cells on the basis of expression of Sca-1 and PDGFR-α, Nature Protocols 7(12) (2012) 2103-2111.
[55] C. Gentili, R. Cancedda, Cartilage and Bone Extracellular Matrix, Current Pharmaceutical Design 15(12) (2009) 1334-1348.

[56] M. Inada, Y. Wang, M.H. Byrne, M.U. Rahman, C. Miyaura, C. López-Otín, S.M. Krane, Critical roles for collagenase-3 (Mmp13) in development of growth plate cartilage and in endochondral ossification, Proc Natl Acad Sci U S A 101(49) (2004) 17192-7.
[57] D. Ferrari, R.A. Kosher, Dlx5 is a positive regulator of chondrocyte differentiation during endochondral ossification, Dev Biol 252(2) (2002) 257-70.
[58] J.Q. Fen, J. Zhang, S.L. Dallas, Y. Lu, S. Chen, X. Tan, M. Owen, S.E. Harris, M. MacDougall, Dentin matrix protein 1, a target molecule for Cbfa1 in bone, is a unique bone marker gene, J Bone Miner Res 17(10) (2002) 1822-31.
[59] V. Agrawal, M. Sinha, A review on carrier systems for bone morphogenetic protein-2, J Biomed Mater Res B Appl Biomater 105(4) (2017) 904-925.
[60] W.G. La, S.W. Kang, H.S. Yang, S.H. Bhang, S.H. Lee, J.H. Park, B.S. Kim, The efficacy of bone morphogenetic protein-2 depends on its mode of delivery, Artif Organs 34(12) (2010) 1150-3.
[61] O. Jeon, S.J. Song, H.S. Yang, S.H. Bhang, S.W. Kang, M.A. Sung, J.H. Lee, B.S. Kim, Long-term delivery enhances in vivo osteogenic efficacy of bone morphogenetic protein-2 compared to short-term delivery, Biochem Biophys Res Commun 369(2) (2008) 774-80.
[62] A.R. Poynton, J.M. Lane, Safety Profile for the Clinical Use of Bone Morphogenetic Proteins in the Spine, Spine 27(16S) (2002).
[63] M. Rodríguez-Évora, A. Delgado, R. Reyes, A. Hernández-Daranas, I. Soriano, J. San Román, C. Évora, Osteogenic effect of local, long versus short term BMP-2 delivery from a novel SPU–PLGA–βTCP concentric system in a critical size defect in rats, European Journal of Pharmaceutical Sciences 49(5) (2013) 873-884.
[64] M.R. Urist, Y.K. Huo, A.G. Brownell, W.M. Hohl, J. Buyske, A. Lietze, P. Tempst, M. Hunkapiller, R.J. DeLange, Purification of bovine bone morphogenetic protein by hydroxyapatite chromatography, Proc Natl Acad Sci U S A 81(2) (1984) 371-5.
[65] X. Dong, Q. Wang, T. Wu, H. Pan, Understanding adsorption-desorption dynamics of BMP-2 on hydroxyapatite (001) surface, Biophys J 93(3) (2007) 750-9.
[66] M.H. Hettiaratchi, L. Krishnan, T. Rouse, C. Chou, T.C. McDevitt, R.E. Guldberg, Heparin-mediated delivery of bone morphogenetic protein-2 improves spatial localization of bone regeneration, Sci Adv 6(1) (2020) eaay1240.
[67] M.H. Hettiaratchi, C. Chou, N. Servies, J.M. Smeekens, A. Cheng, C. Esancy, R. Wu, T.C. McDevitt, R.E. Guldberg, L. Krishnan, Competitive Protein Binding Influences Heparin-Based Modulation of Spatial Growth Factor Delivery for Bone Regeneration, Tissue Eng Part A 23(13-14) (2017) 683-695.
[68] A. Shekaran, J.R. García, A.Y. Clark, T.E. Kavanaugh, A.S. Lin, R.E. Guldberg, A.J. García, Bone regeneration using an alpha 2 beta 1 integrin-specific hydrogel as a BMP-2 delivery vehicle, Biomaterials 35(21) (2014) 5453-61.
[69] J.D. Boerckel, Y.M. Kolambkar, K.M. Dupont, B.A. Uhrig, E.A. Phelps, H.Y. Stevens, A.J. García, R.E. Guldberg, Effects of protein dose and delivery system on BMP-mediated bone regeneration, Biomaterials 32(22) (2011) 5241-51.
[70] J.D. Boerckel, Y.M. Kolambkar, H.Y. Stevens, A.S. Lin, K.M. Dupont, R.E. Guldberg, Effects of in vivo mechanical loading on large bone defect regeneration, J Orthop Res 30(7) (2012) 1067-75.
[71] S. Herberg, A.M. McDermott, P.N. Dang, D.S. Alt, R. Tang, J.H. Dawahare, D. Varghai, J.-Y. Shin, A. McMillan, A.D. Dikina, F. He, Y.B. Lee, Y. Cheng, K. Umemori, P.C. Wong, H. Park, J.D. Boerckel, E. Alsberg, Combinatorial morphogenetic and mechanical cues to mimic bone development for defect repair, Science Advances 5(8) (2019) eaax2476.

[72] B.S. Klosterhoff, C.E. Vantucci, J. Kaiser, K.G. Ong, L.B. Wood, J.A. Weiss, R.E. Guldberg, N.J. Willett, Effects of osteogenic ambulatory mechanical stimulation on early stages of BMP-2 mediated bone repair, Connect Tissue Res 63(1) (2022) 16-27.
[73] J.D. Boerckel, K.M. Dupont, Y.M. Kolambkar, A.S. Lin, R.E. Guldberg, In vivo model for evaluating the effects of mechanical stimulation on tissue-engineered bone repair, J Biomech Eng 131(8) (2009) 084502.
[74] M. Windolf, M. Ernst, R. Schwyn, D. Arens, S. Zeiter, The relation between fracture activity and bone healing with special reference to the early healing phase - A preclinical study, Injury 52(1) (2021) 71-77.
[75] F.D.A, Summary of Safety and Effectiveness Data, 2002. https://www.accessdata.fda.gov/cdrh_docs/pdf/p000058b.pdf. (Accessed 4th February 2023).
[76] A. Mesfin, J.M. Buchowski, L.P. Zebala, W.R. Bakhsh, A.B. Aronson, J.L. Fogelson, S. Hershman, H.J. Kim, A. Ahmad, K.H. Bridwell, High-dose rhBMP-2 for adults: major and minor complications: a study of 502 spine cases, J Bone Joint Surg Am 95(17) (2013) 1546-53.
[77] T. Yoshii, M. Hashimoto, S. Egawa, T. Hirai, H. Inose, A. Okawa, Hydroxyapatite/collagen composite graft for posterior lumbar interbody fusion: a comparison with local bone graft, J Orthop Surg Res 16(1) (2021) 639.
[78] X. Wei, S. Egawa, R. Matsumoto, H. Yasuda, K. Hirai, T. Yoshii, A. Okawa, T. Nakajima, S. Sotome, Augmentation of fracture healing by hydroxyapatite/collagen paste and bone morphogenetic protein-2 evaluated using a rat femur osteotomy model, J Orthop Res 36(1) (2018) 129-137.
[79] M.J. Meagher, H.E. Weiss-Bilka, M.E. Best, J.D. Boerckel, D.R. Wagner, R.K. Roeder, Acellular hydroxyapatite-collagen scaffolds support angiogenesis and osteogenic gene expression in an ectopic murine model: Effects of hydroxyapatite volume fraction, J Biomed Mater Res A 104(9) (2016) 2178-88.
[80] R.J. Kane, H.E. Weiss-Bilka, M.J. Meagher, Y. Liu, J.A. Gargac, G.L. Niebur, D.R. Wagner, R.K. Roeder, Hydroxyapatite reinforced collagen scaffolds with improved architecture and mechanical properties, Acta Biomater 17 (2015) 16-25.
[81] S.A. Mindea, P. Shih, J.K. Song, Recombinant human bone morphogenetic protein-2-induced radiculitis in elective minimally invasive transforaminal lumbar interbody fusions: a series review, Spine (Phila Pa 1976) 34(14) (2009) 1480-4; discussion 1485.
[82] P. Haubruck, M.C. Tanner, W. Vlachopoulos, S. Hagelskamp, M. Miska, J. Ober, C. Fischer, G. Schmidmaier, Comparison of the clinical effectiveness of Bone Morphogenic Protein (BMP) -2 and -7 in the adjunct treatment of lower limb nonunions, Orthopaedics & Traumatology: Surgery & Research 104(8) (2018) 1241-1248.

Statement of significance

- Incorporation of hydroxyapatite (HA) in a collagen scaffold dramatically improves bone morphogenic protein (BMP) sequestration via biophysical interactions with BMP, thereby providing more controlled BMP release compared with pristine collagen.

- We then investigate the molecular mechanisms responsible for increased osteoinductive potential of a heterodimer BMP-2/7 with is clinically used counterpart, the BMP-2 homodimer.

- The superior osteoinductive properties of BMP-2/7 are a consequence of its direct positive effect on progenitor cell homing at the implantation site, which consequently leads to upregulation of cartilage and bone related genes and biochemical markers.

- An ultra-low dose of BMP-2/7 delivered via a collagen-HA (CHA) scaffold leads to accelerated healing of a critical femoral defect in rats while a 20-times higher BMP-2 dose was required to achieve comparable results.

Graphical Abstract

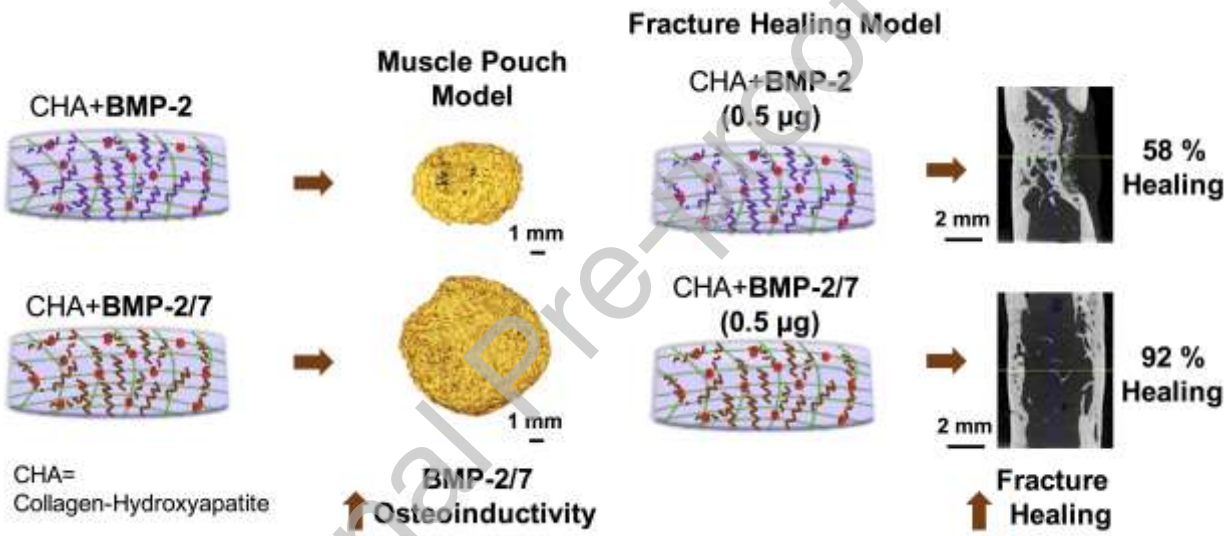

Declaration of interests

☐The authors declare that they have no known competing financial interests or personal relationships that could have appeared to influence the work reported in this paper.

☒The authors declare the following financial interests/personal relationships which may be considered as potential competing interests:

Deepak Bushan Raina reports financial support was provided by Maggie-Stephens Foundation. Deepak Bushan Raina reports financial support was provided by Sten K Johnson Foundation. Deepak Bushan Raina reports financial support was provided by Crafoord Foundation. Fergal J O'Brien reports financial support was provided by Health Research Board. Fergal J O'Brien reports financial support was provided by European Research Council. Fergal J O'Brien reports financial support was provided by EU BlueHuman Interreg Atlantic Area Project. Deepak Bushan Raina reports a relationship with Moroxite AB that includes: equity or stocks. Deepak Bushan Raina reports a relationship with Moroxite F AB that includes: equity or stocks. Fergal J O'Brien has patent issued to Locate Bio.